

## Mariner 6 and 7 Ultraviolet Spectrometer Experiment: Photometry and Topography of Mars

CHARLES W. HORD

*Department of Astro-Geophysics and Laboratory for Atmospheric and Space Physics,  
University of Colorado, Boulder, Colorado 80302*

Received September 27, 1971

From data obtained by the ultraviolet spectrometers aboard the Mariner 6 and 7 Mars missions the reflectivity of the illuminated disk of Mars was found to have two distinct spectral types, associated with polar and nonpolar regions. In this work the characteristic spectrum of nonpolar regions on Mars is discussed. An interpretation of the variation of the intensity at 3050 Å due to surface pressure variations is given. A comparison of the ultraviolet observations with pressures inferred by the infrared spectrometer is used to test this interpretation and to determine physical parameters of Mars which lead to the observed reflectance. Earth based pressures obtained by broadening of the  $1\mu$  band of CO<sub>2</sub> and radar topography are compared with the ultraviolet results.

### INTRODUCTION

In 1969 the Mariner 6 and 7 spacecraft swept past Mars on the afternoon side of the planet obtaining spectroscopic and imaging data of high spatial resolution. The ultraviolet spectrometers aboard the Mariner spacecraft obtained information about the make-up of the Mars atmosphere based upon emission spectra from the uppermost part of the atmosphere (Barth *et al.*, 1969, 1971). In addition, over 400 spectra were obtained of the illuminated disk of Mars. Of these disk spectra, about 40 were obtained while viewing the southern polar cap. Initial analysis of the polar cap spectra shows a distinctive absorption feature at 2550 Å which is most simply explained by the presence of  $1 \times 10^{-3}$  cm-atm of ozone which gives the observed absorption optical depth,  $\tau$  (2550 Å) = 0.3, (Barth and Hord, 1971). None of the nonpolar spectra shows this absorption feature, which is present in all 40 polar spectra. The photometric properties found from the ultraviolet polar data have been discussed by Pang and Hord (1971).

In this work the photometric properties of the nonpolar or desert regions of Mars are discussed. Specifically considered is the

photometric model at wavelengths shorter than 3500 Å. Initial analysis has shown that wavelengths longer than 3500 Å have different photometric properties which will not be discussed here.

### DATA

The long wavelength channel of the Mariner ultraviolet spectrometers obtained one spectrum every three seconds in the 1900-4300 Å range at 20 Å resolution (Pearce *et al.*, 1971). An instrument field of view of  $0^{\circ}23 \times 2^{\circ}3$  gave spatial resolution which varied from about  $30 \times 300$  km near the bright limb to  $14 \times 140$  km at the closest approach of the spacecraft. The long axis of the projected field of view was oriented perpendicular to the solar direction.

In analyzing the spectrometer data it was found that only small changes in spectral shape occur shortward of 3500 Å. This means that the general photometric properties in this wavelength region are relatively wavelength independent. In order to describe the photometric function, the intensity or reflectance measurements in a 100 Å wavelength band centered at 3050 Å are analyzed. The photometric properties deduced are representative of

the wavelength region from 2600 Å to about 3500 Å. Second order changes in spectral shape, which do occur, are felt to be due to varying atmospheric opacity at the shorter wavelengths and the increase in ground albedo contribution at longer wavelengths. Using the intensity sum over a 100 Å wavelength interval gives relative measurements to an accuracy better than 1%. Absolute intensities are limited by our knowledge of the solar flux and the instrument calibration (Pearce *et al.*, 1971).

#### PHOTOMETRIC MEASUREMENTS

Reflectance properties of Mars at 3050 Å measured by Mariner 6 and 7 are shown in Figs. 1, 2, and 3. Reflectance is defined as

$$R = \pi B/F, \quad (1)$$

where  $B$  is the measured intensity, or surface brightness, and  $F$  is the solar flux at Mars. These figures show data taken at phase angles ranging from 46° to 91° as the instrument field of view swept from the bright limb across the afternoon side of the planet toward the terminator. Also plotted are the cosine of the emission angle,  $\mu$ , and cosine of the incidence angle,  $\mu_0$ , which have their usual radiative transfer meaning (Chandrasekhar, 1960) with emission angle defined as the angle between observed emitted radiation and the local normal, and the incidence angle defined as the angle between the Sun and local normal. The base maps used here show the ultraviolet observation swath across Mars in the combined context of Mariner television pictures (e.g., Leighton *et al.*, 1969) and a classical map of Mars. Mariner 6 data, shown in Fig. 1, are for regions extending from north of Juventae Fons to Aurorae Sinus and from Chryse to the west edge of Meridiani Sinus. Mariner 6 data, shown in Fig. 2, are for a region south of Margaritifer Sinus extending from Pyrrhae Regio to Deucalionis Regio. In the Mariner 7 case, shown in Fig. 3, ultraviolet observations extend from south of Nectar across the Argyre 1 region toward the polar cap, and from the Pandorae Fretum region across Noachis and Hellespontus into Hellas. A tabular listing of data shown in Figs. 1, 2,

and 3 is included in Table I along with latitude and longitude values.

In order to compare these measurements with Earth-based measurements it is useful to find parameters  $k$  and  $R_0$  that provide a best fit of the Minnaert function

$$R = R_0 \mu_0^k \mu^{k-1} \quad (2)$$

to the 3050 Å reflectance (Minnaert, 1941). A recent discussion of the properties of this function and its application to Mariner 6 and 7 television data is given by Young and Collins (1971).

It is important to note that the ultraviolet location being observed on Mars is changing throughout the measurements. Even though Mars shows relatively small contrast in the ultraviolet, the albedo may be varying. In order to make a more nearly valid application of Minnaert's law to these data, regions can be selected which have a nearly uniform albedo at visible wavelengths. Using the Mercator photomap of Mars prepared by Cutts *et al.* (1971) from Mariner 6 and 7 television data and the 1969 Mars map prepared by Lowell Observatory (Inge *et al.*, 1971), four regions having nearly uniform albedo were selected for analysis.

Consider first Mariner 6 data obtained at a phase angle of 91°. In the Aurorae Sinus, Margaritifer Sinus region extending from a latitude and longitude of -12°7, 42°7 to -15°9, 18°8 the Minnaert parameters were  $k = 0.71 \pm 0.02$  and  $R_0 = 0.037$ . For the Deucalionis Regio region south of Meridiani Sinus in the latitude and longitude range from -17°8, 357°7 to -17°5, 349°1 the Minnaert parameters were  $k = 0.69 \pm 0.06$  and  $R_0 = 0.031$ . The Mariner 7 data obtained at a phase angle of 91° covered two regions of nearly uniform visual albedo. One of these regions extending from Deucalionis Regio across Pandorae Fretum toward Hellespontus covering the latitude and longitude range from -19°8, 353°8 to -37°9, 331°0 gives  $k = 0.31 \pm 0.01$  and  $R_0 = 0.022$ . This region appears uniform on the Lowell map; however, the Mercator photomap based upon Mariner television pictures indicates a slight decrease in albedo approaching Hellespontus. This decrease in albedo could account for the

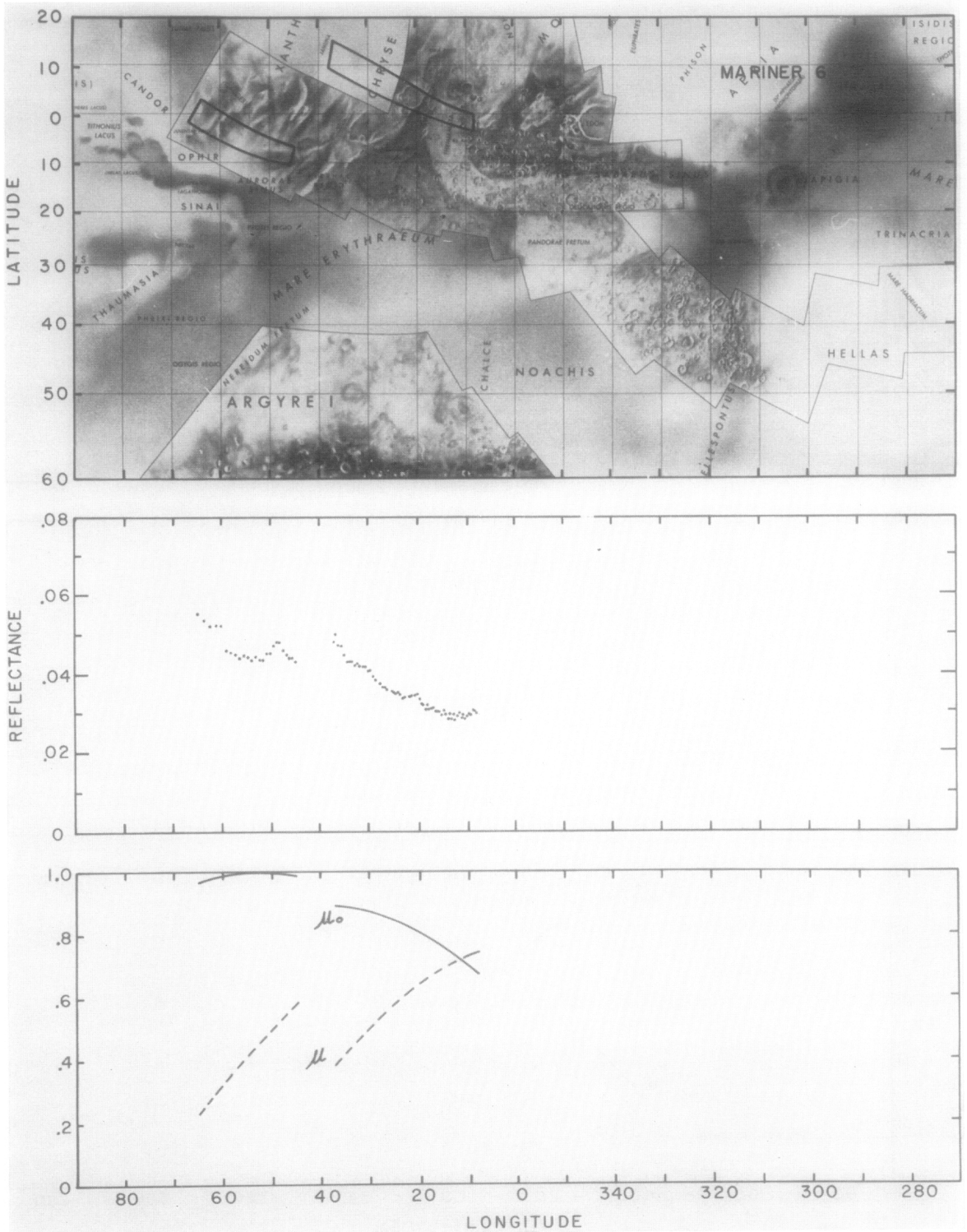


FIG. 1. Mariner 6 reflectance measurements at 3050 Å. The top part of the figure shows a projection of the ultraviolet spectrometer field of view on a map prepared by the Army Topographic Service. This map displays an early version of the Mariner 6 and 7 television pictures in the context of a classical map of Mars. Reflectance and the cosines of the incidence and emission angles,  $\mu_0$  and  $\mu$ , are given as a function of longitude. These data were obtained at a phase angle of 62°.

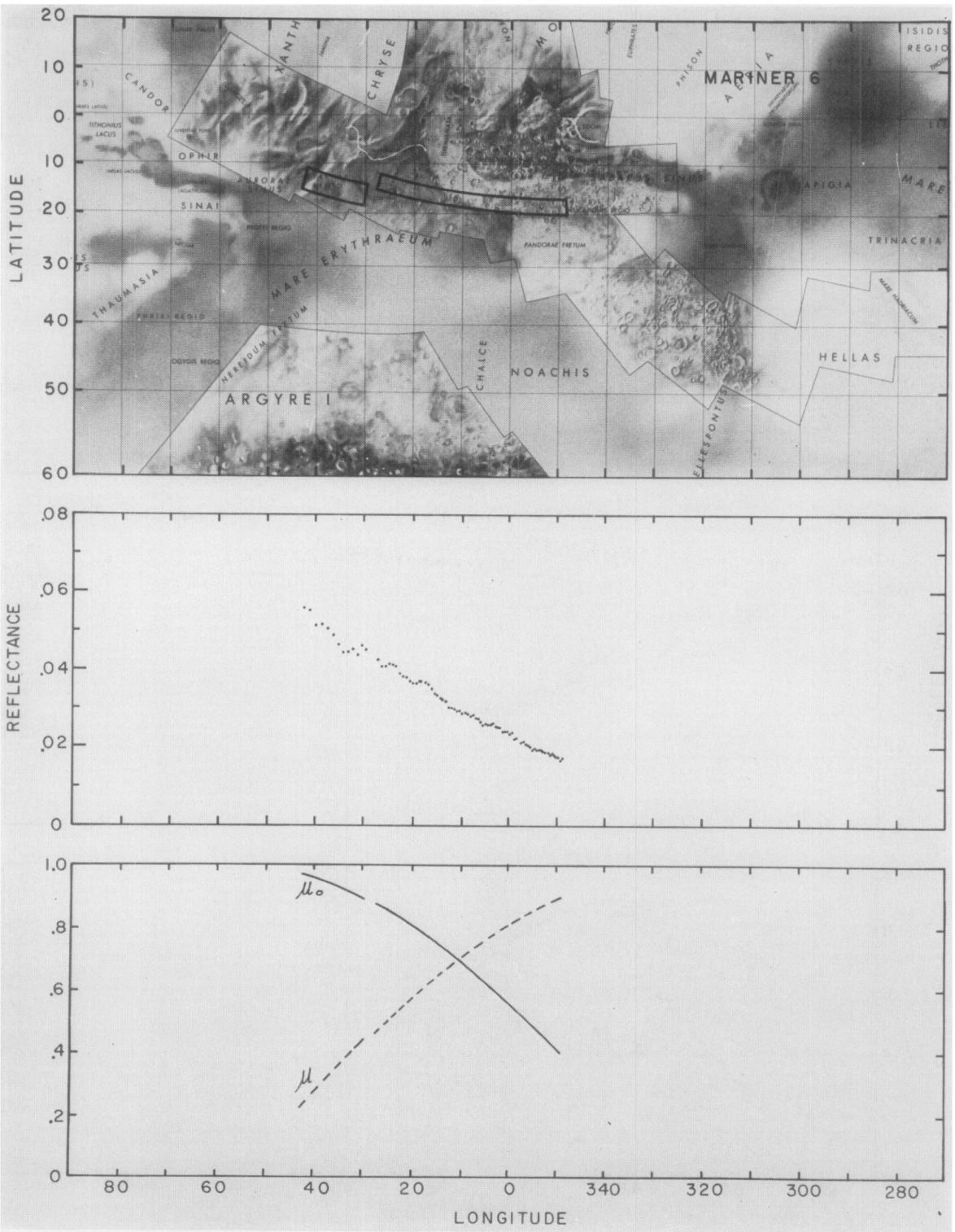


FIG. 2. Mariner 6 reflectance measurements at 3050 Å obtained at a phase angle of 91°.

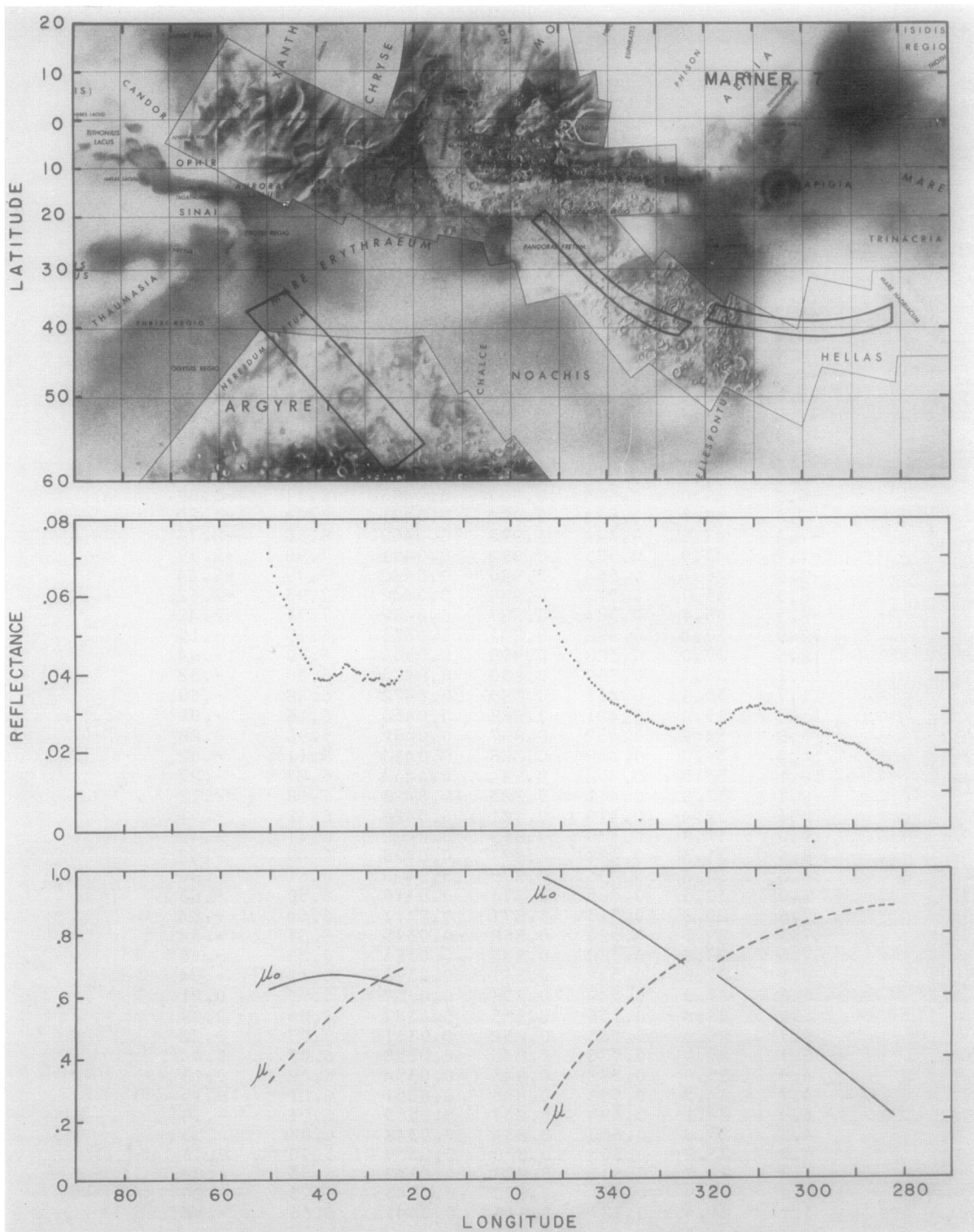


FIG. 3. Mariner 7 reflectance measurements at  $0.050 \text{ \AA}$ . Data in the left-hand swath were obtained at a phase angle of  $46^\circ$  and at  $91^\circ$  in the two swaths on the right.

TABLE I

Mariner 6, Phase Angle = 62.5

Lat.	Lon.	$\mu$	$\mu_0$	R	Pres.	Alt.
1.2	65.2	0.230	0.969	0.0555	4.36	3.36
0.5	63.8	0.257	0.975	0.0537	4.64	2.74
-.2	62.5	0.281	0.980	0.0523	4.89	2.21
-.8	61.4	0.303	0.984	0.0525	5.32	1.38
-1.4	60.3	0.324	0.988	0.0524	5.67	0.73
-1.9	59.3	0.343	0.990	0.0461	4.89	2.22
-2.4	58.3	0.361	0.993	0.0456	5.06	1.86
-2.9	57.4	0.378	0.994	0.0451	5.21	1.58
-3.3	56.5	0.394	0.996	0.0441	5.24	1.52
-3.7	55.6	0.409	0.997	0.0448	5.61	0.85
-4.1	54.8	0.424	0.998	0.0444	5.73	0.64
-4.5	54.0	0.438	0.998	0.0436	5.75	0.59
-4.9	53.2	0.451	0.998	0.0446	6.18	-.13
-5.3	52.5	0.464	0.998	0.0437	6.14	-.07
-5.6	51.7	0.477	0.998	0.0437	6.34	-.39
-5.9	51.0	0.489	0.998	0.0454	6.95	-1.30
-6.3	50.3	0.501	0.997	0.0455	7.16	-1.60
-6.6	49.6	0.512	0.996	0.0473	7.84	-2.50
-6.9	49.0	0.523	0.995	0.0483	8.31	-3.09
-7.2	48.3	0.534	0.994	0.0481	8.44	-3.25
-7.4	47.6	0.544	0.993	0.0462	8.06	-2.78
-7.7	47.0	0.555	0.992	0.0451	7.90	-2.59
-8.0	46.4	0.564	0.990	0.0442	7.79	-2.44
-8.3	45.7	0.574	0.989	0.0442	7.93	-2.62
-8.5	45.1	0.584	0.987	0.0432	7.77	-2.42
12.9	37.4	0.382	0.891	0.0483	6.19	-.15
12.6	37.0	0.388	0.890	0.0502	6.70	-.94
12.1	36.4	0.399	0.890	0.0473	6.30	-.32
11.7	35.8	0.411	0.889	0.0472	6.48	-.60
11.3	35.2	0.421	0.888	0.0450	6.16	-.09
10.8	34.6	0.432	0.887	0.0432	5.93	0.28
10.4	34.0	0.442	0.886	0.0433	6.11	-.02
10.1	33.5	0.452	0.884	0.0434	6.27	-.27
9.7	32.9	0.461	0.883	0.0423	6.18	-.12
9.3	32.4	0.470	0.881	0.0428	6.42	-.51
9.0	31.8	0.479	0.879	0.0422	6.41	-.49
8.6	31.3	0.488	0.877	0.0420	6.49	-.62
8.3	30.8	0.496	0.875	0.0420	6.61	-.80
8.0	30.3	0.505	0.873	0.0410	6.50	-.63
7.6	29.8	0.513	0.871	0.0411	6.64	-.84
7.3	29.3	0.520	0.868	0.0395	6.31	-.34
7.0	28.8	0.528	0.866	0.0386	6.20	-.16
6.5	27.8	0.542	0.861	0.0376	6.12	-.04
6.2	27.3	0.549	0.858	0.0367	5.97	0.21
5.9	26.8	0.556	0.855	0.0367	6.05	0.09
5.7	26.4	0.563	0.852	0.0361	5.97	0.22
5.1	25.5	0.576	0.846	0.0358	6.07	0.06
4.9	25.0	0.582	0.843	0.0354	6.02	0.13
4.7	24.5	0.588	0.840	0.0351	6.01	0.15
4.4	24.1	0.594	0.837	0.0355	6.21	-.18
4.2	23.6	0.600	0.834	0.0348	6.08	0.03
4.0	23.2	0.605	0.830	0.0339	5.90	0.33
3.8	22.7	0.611	0.827	0.0342	6.06	0.08
3.3	21.9	0.621	0.820	0.0343	6.23	-.20
3.1	21.4	0.627	0.816	0.0345	6.36	-.42

TABLE I *continued*  
 Mariner 6, Phase Angle = 62.5

Lat.	Lon.	$\mu$	$\mu_0$	R	Pres.	Alt.
2.7	20.6	0.637	0.809	0.0347	6.58	-.75
2.5	20.1	0.641	0.805	0.0349	6.73	-.98
2.4	19.7	0.646	0.802	0.0338	6.42	-.51
2.2	19.3	0.651	0.798	0.0325	6.07	0.05
2.0	18.9	0.655	0.794	0.0322	6.04	0.10
1.8	18.5	0.660	0.790	0.0310	5.71	0.66
1.6	18.0	0.664	0.786	0.0323	6.21	-.18
1.5	17.6	0.668	0.782	0.0311	5.88	0.38
1.3	17.2	0.672	0.778	0.0313	5.98	0.21
1.1	16.8	0.676	0.774	0.0315	6.13	-.04
1.0	16.4	0.680	0.770	0.0306	5.88	0.37
0.8	16.0	0.684	0.766	0.0305	5.91	0.33
0.7	15.6	0.688	0.761	0.0304	5.93	0.29
0.5	15.1	0.691	0.757	0.0296	5.71	0.67
0.4	14.7	0.695	0.753	0.0308	6.17	-.12
0.2	14.3	0.698	0.749	0.0297	5.84	0.45
0.1	13.9	0.702	0.744	0.0285	5.47	1.10
-.0	13.5	0.705	0.740	0.0300	6.07	0.06
-.2	13.1	0.708	0.735	0.0287	5.65	0.77
-.3	12.7	0.711	0.731	0.0299	6.13	-.04
-.4	12.3	0.714	0.726	0.0284	5.63	0.80
-.5	11.9	0.717	0.722	0.0295	6.10	0.00
-.7	11.5	0.720	0.717	0.0303	6.42	-.51
-.8	11.1	0.723	0.712	0.0289	5.97	0.22
-.9	10.7	0.726	0.708	0.0298	6.34	-.38
-1.0	10.3	0.729	0.703	0.0286	5.97	0.22
-1.1	9.9	0.731	0.698	0.0293	6.26	-.26
-1.2	9.6	0.734	0.694	0.0300	6.57	-.74
-1.3	9.2	0.736	0.689	0.0298	6.55	-.70
-1.4	8.8	0.739	0.684	0.0309	7.04	-1.43
-1.5	8.4	0.741	0.679	0.0307	7.01	-1.38
-1.6	8.0	0.743	0.674	0.0302	6.87	-1.18

Mariner 6, Phase Angle = 90.9

-12.7	42.7	0.224	0.971	0.0559	3.97	4.29
-13.1	41.6	0.243	0.966	0.0552	4.26	3.60
-13.5	40.3	0.266	0.960	0.0514	4.20	3.74
-13.9	39.0	0.288	0.953	0.0516	4.60	2.84
-14.3	37.8	0.309	0.946	0.0505	4.79	2.42
-14.6	36.7	0.328	0.939	0.0488	4.85	2.29
-15.0	35.6	0.346	0.933	0.0464	4.77	2.46
-15.3	34.5	0.364	0.926	0.0444	4.69	2.64
-15.5	33.5	0.380	0.919	0.0446	4.98	2.04
-15.8	32.5	0.396	0.912	0.0452	5.32	1.37
-16.1	31.6	0.411	0.905	0.0437	5.26	1.48
-16.3	30.7	0.425	0.898	0.0462	6.00	0.18
-16.5	29.8	0.440	0.891	0.0451	5.99	0.19
-14.0	27.4	0.458	0.877	0.0425	5.74	0.61
-14.2	26.5	0.471	0.869	0.0408	5.55	0.94
-14.4	25.8	0.483	0.863	0.0408	5.74	0.61

TABLE I *continued*  
 Mariner 6, Phase Angle = 90.9

Lat.	Lon.	$\mu$	$\mu_0$	R	Pres.	Alt.
-14.6	25.0	0.495	0.856	0.0415	6.08	0.04
-14.8	24.3	0.506	0.849	0.0412	6.18	-.12
-14.9	23.5	0.517	0.842	0.0408	6.24	-.22
-15.1	22.8	0.528	0.835	0.0390	5.94	0.26
-15.2	22.1	0.538	0.828	0.0381	5.87	0.39
-15.4	21.4	0.548	0.822	0.0379	5.95	0.25
-15.5	20.8	0.558	0.815	0.0369	5.83	0.45
-15.7	20.1	0.567	0.808	0.0364	5.85	0.42
-15.8	19.4	0.577	0.801	0.0364	5.97	0.22
-15.9	18.8	0.586	0.794	0.0369	6.24	-.22
-16.0	18.4	0.591	0.790	0.0369	6.33	-.36
-16.1	17.5	0.603	0.781	0.0367	6.45	-.56
-16.3	16.9	0.612	0.774	0.0362	6.42	-.51
-16.4	16.3	0.620	0.767	0.0350	6.19	-.14
-16.5	15.6	0.628	0.760	0.0338	5.97	0.22
-16.5	15.0	0.636	0.753	0.0333	5.95	0.26
-16.6	14.4	0.644	0.746	0.0325	5.81	0.49
-16.7	13.8	0.652	0.740	0.0322	5.82	0.48
-16.8	13.3	0.659	0.733	0.0317	5.77	0.56
-16.9	12.7	0.666	0.726	0.0301	5.37	1.27
-17.0	12.1	0.674	0.719	0.0301	5.48	1.07
-17.0	11.5	0.681	0.712	0.0298	5.48	1.08
-17.1	11.0	0.688	0.706	0.0292	5.37	1.27
-17.2	10.4	0.694	0.699	0.0294	5.53	0.99
-17.2	9.9	0.701	0.692	0.0287	5.41	1.21
-17.3	9.3	0.708	0.685	0.0289	5.55	0.96
-17.3	8.8	0.714	0.678	0.0285	5.50	1.04
-17.4	8.2	0.720	0.671	0.0280	5.41	1.20
-17.4	7.7	0.726	0.665	0.0283	5.62	0.83
-17.5	7.1	0.732	0.658	0.0275	5.43	1.18
-17.5	6.6	0.738	0.651	0.0273	5.45	1.14
-17.5	6.1	0.744	0.644	0.0265	5.25	1.50
-17.6	5.6	0.750	0.637	0.0257	5.07	1.85
-17.6	5.1	0.756	0.630	0.0262	5.32	1.37
-17.6	4.5	0.761	0.624	0.0259	5.28	1.45
-17.7	4.0	0.766	0.617	0.0259	5.36	1.30
-17.7	3.5	0.772	0.610	0.0261	5.52	1.00
-17.7	3.0	0.777	0.603	0.0253	5.31	1.39
-17.7	2.5	0.782	0.596	0.0252	5.34	1.34
-17.8	2.0	0.787	0.589	0.0251	5.38	1.26
-17.8	1.5	0.792	0.583	0.0240	5.05	1.90
-17.8	1.0	0.797	0.576	0.0242	5.22	1.57
-17.8	0.5	0.802	0.569	0.0241	5.24	1.52
-17.8	0.1	0.806	0.562	0.0235	5.10	1.80
-17.8	359.6	0.811	0.555	0.0238	5.26	1.49
-17.8	359.1	0.816	0.548	0.0222	4.76	2.48
-17.8	358.6	0.820	0.542	0.0224	4.89	2.22
-17.8	357.7	0.828	0.528	0.0212	4.58	2.86
-17.8	357.2	0.833	0.521	0.0215	4.76	2.49
-17.8	356.7	0.837	0.514	0.0208	4.57	2.90
-17.8	356.3	0.841	0.508	0.0205	4.51	3.03
-17.8	355.8	0.845	0.501	0.0201	4.41	3.25
-17.8	355.3	0.849	0.494	0.0194	4.20	3.73
-17.8	354.9	0.853	0.487	0.0197	4.38	3.32
-17.8	354.4	0.856	0.480	0.0193	4.29	3.54
-17.8	354.0	0.860	0.473	0.0195	4.44	3.17

TABLE I *continued*  
 Mariner 6, Phase Angle = 90.9

Lat.	Lon.	$\mu$	$\mu_0$	R	Pres.	Alt.
-17.7	353.5	0.864	0.467	0.0194	4.44	3.17
-17.7	353.1	0.867	0.460	0.0190	4.37	3.33
-17.7	352.6	0.871	0.453	0.0187	4.31	3.48
-17.7	352.2	0.874	0.446	0.0186	4.34	3.41
-17.6	351.7	0.878	0.439	0.0180	4.14	3.88
-17.6	351.3	0.881	0.432	0.0184	4.36	3.37
-17.6	350.8	0.884	0.426	0.0180	4.28	3.54
-17.6	350.4	0.887	0.419	0.0176	4.17	3.80
-17.5	350.0	0.890	0.412	0.0175	4.18	3.79
-17.5	349.5	0.893	0.405	0.0167	3.92	4.42
-17.5	349.1	0.896	0.398	0.0174	4.27	3.57

Mariner 7, Phase Angle = 46.3

-35.6	50.4	0.317	0.615	0.0711	7.49	-2.04
-36.2	49.7	0.330	0.620	0.0678	7.31	-1.81
-36.8	49.0	0.343	0.624	0.0652	7.21	-1.67
-37.4	48.3	0.355	0.628	0.0623	7.01	-1.39
-37.9	47.7	0.367	0.632	0.0605	6.96	-1.32
-38.5	47.1	0.378	0.635	0.0592	6.98	-1.34
-39.0	46.5	0.389	0.639	0.0577	6.92	-1.25
-39.5	45.9	0.400	0.641	0.0555	6.73	-.98
-40.0	45.3	0.410	0.644	0.0528	6.44	-.53
-40.5	44.7	0.420	0.646	0.0501	6.13	-.04
-41.0	44.2	0.429	0.648	0.0480	5.90	0.33
-41.5	43.6	0.438	0.650	0.0462	5.70	0.68
-42.0	43.1	0.447	0.652	0.0451	5.62	0.82
-42.4	42.6	0.456	0.654	0.0440	5.54	0.97
-42.9	42.1	0.464	0.655	0.0430	5.45	1.13
-43.3	41.6	0.472	0.656	0.0414	5.25	1.50
-43.8	41.0	0.480	0.658	0.0389	4.88	2.24
-44.2	40.5	0.488	0.658	0.0388	4.95	2.10
-44.6	40.1	0.495	0.659	0.0389	5.04	1.90
-45.1	39.6	0.503	0.660	0.0386	5.06	1.88
-45.5	39.1	0.510	0.661	0.0387	5.16	1.67
-45.9	38.6	0.517	0.661	0.0385	5.19	1.63
-46.3	38.1	0.524	0.661	0.0385	5.27	1.47
-46.7	37.6	0.530	0.662	0.0387	5.37	1.27
-47.1	37.2	0.537	0.662	0.0392	5.55	0.94
-47.5	36.7	0.543	0.662	0.0401	5.83	0.46
-47.9	36.2	0.549	0.662	0.0397	5.80	0.50
-48.2	35.8	0.556	0.661	0.0401	5.98	0.21
-48.6	35.3	0.562	0.661	0.0405	6.13	-.04
-49.0	34.9	0.567	0.661	0.0417	6.46	-.57
-49.4	34.4	0.573	0.660	0.0425	6.72	-.97
-49.7	33.9	0.579	0.660	0.0425	6.81	-1.09
-50.1	33.5	0.584	0.659	0.0421	6.77	-1.04
-50.5	33.0	0.589	0.658	0.0413	6.67	-.88
-50.8	32.6	0.595	0.658	0.0409	6.64	-.85
-51.2	32.1	0.600	0.657	0.0405	6.61	-.80
-51.5	31.7	0.605	0.656	0.0406	6.69	-.92
-51.9	31.2	0.610	0.655	0.0403	6.67	-.88
-52.2	30.8	0.614	0.654	0.0386	6.32	-.35

TABLE I *continued*  
 Mariner 7, Phase Angle = 46.3

Lat.	Lon.	$\mu$	$\mu_0$	R	Pres.	Alt.
-52.6	30.3	0.619	0.653	0.0390	6.47	-.59
-52.9	29.9	0.624	0.651	0.0400	6.80	-1.08
-53.3	29.4	0.628	0.650	0.0388	6.53	-.68
-53.6	29.0	0.633	0.649	0.0385	6.53	-.68
-53.9	28.5	0.637	0.647	0.0386	6.60	-.78
-54.3	28.0	0.641	0.646	0.0389	6.73	-.98
-54.6	27.6	0.645	0.645	0.0390	6.81	-1.10
-54.9	27.1	0.649	0.643	0.0375	6.48	-.59
-55.3	26.7	0.653	0.641	0.0374	6.49	-.61
-55.6	26.2	0.657	0.640	0.0370	6.44	-.53
-55.9	25.8	0.661	0.638	0.0375	6.62	-.81
-56.2	25.3	0.665	0.636	0.0375	6.67	-.89
-56.6	24.8	0.668	0.634	0.0383	6.94	-1.29
-56.9	24.4	0.672	0.632	0.0376	6.80	-1.08
-57.2	23.9	0.676	0.630	0.0384	7.08	-1.48
-57.5	23.4	0.679	0.628	0.0395	7.42	-1.95
-57.8	22.9	0.682	0.626	0.0407	7.80	-2.46

Mariner 7, Phase Angle = 90.7

-19.8	353.8	0.225	0.971	0.0588	4.31	3.49
-20.4	353.2	0.238	0.968	0.0574	4.42	3.23
-21.4	352.3	0.260	0.962	0.0549	4.53	2.98
-22.3	351.5	0.281	0.956	0.0523	4.57	2.88
-23.3	350.6	0.301	0.949	0.0503	4.64	2.74
-24.1	349.8	0.320	0.943	0.0481	4.62	2.79
-24.9	349.0	0.338	0.936	0.0461	4.58	2.86
-25.7	348.2	0.355	0.929	0.0445	4.58	2.86
-26.4	347.4	0.371	0.923	0.0433	4.61	2.80
-27.1	346.7	0.387	0.916	0.0420	4.61	2.81
-28.4	345.2	0.416	0.903	0.0401	4.63	2.76
-29.0	344.5	0.429	0.896	0.0387	4.53	2.98
-29.6	343.9	0.443	0.890	0.0376	4.49	3.07
-30.2	343.2	0.455	0.883	0.0369	4.49	3.06
-30.7	342.5	0.467	0.876	0.0360	4.44	3.18
-31.2	341.8	0.479	0.870	0.0351	4.40	3.28
-31.7	341.2	0.491	0.863	0.0344	4.37	3.35
-32.2	340.5	0.502	0.856	0.0336	4.31	3.48
-32.7	339.8	0.512	0.850	0.0327	4.22	3.68
-33.1	339.2	0.523	0.843	0.0324	4.27	3.58
-33.6	338.6	0.533	0.836	0.0320	4.30	3.49
-34.0	337.9	0.543	0.830	0.0312	4.20	3.73
-34.4	337.3	0.553	0.823	0.0316	4.40	3.27
-34.8	336.6	0.562	0.816	0.0304	4.22	3.69
-35.2	336.0	0.571	0.810	0.0303	4.29	3.52
-35.6	335.4	0.580	0.803	0.0298	4.26	3.60
-35.9	334.8	0.589	0.797	0.0291	4.17	3.81
-36.3	334.1	0.597	0.790	0.0294	4.34	3.41
-36.6	333.5	0.606	0.783	0.0282	4.10	3.97
-37.0	332.9	0.614	0.777	0.0280	4.14	3.87
-37.3	332.3	0.622	0.770	0.0283	4.30	3.50
-37.6	331.6	0.630	0.763	0.0276	4.21	3.72
-37.9	331.0	0.637	0.757	0.0272	4.17	3.81

TABLE I *continued*

Mariner 7, Phase Angle = 90.7

Lat.	Lon.	$\mu$	$\mu_0$	R	Pres.	Alt.
-38.2	330.4	0.645	0.750	0.0268	4.13	3.90
-38.5	329.8	0.652	0.744	0.0264	4.09	4.01
-38.8	329.2	0.659	0.737	0.0265	4.20	3.73
-39.1	328.5	0.666	0.730	0.0260	4.12	3.93
-39.3	327.9	0.673	0.724	0.0258	4.15	3.85
-39.6	327.3	0.680	0.717	0.0260	4.27	3.58
-39.8	326.7	0.686	0.710	0.0260	4.37	3.35
-40.1	326.1	0.693	0.704	0.0266	4.62	2.78
-40.3	325.5	0.699	0.697	0.0259	4.47	3.11
-40.6	324.9	0.705	0.691	0.0264	4.69	2.64
-36.5	318.0	0.695	0.651	0.0271	5.04	1.92
-36.7	317.4	0.700	0.644	0.0266	4.95	2.09
-36.9	316.8	0.706	0.637	0.0271	5.17	1.66
-37.1	316.3	0.711	0.631	0.0273	5.31	1.38
-37.2	315.7	0.716	0.624	0.0280	5.63	0.81
-37.4	315.2	0.721	0.618	0.0285	5.88	0.37
-37.5	314.6	0.725	0.611	0.0297	6.37	-0.42
-37.7	314.0	0.730	0.604	0.0306	6.75	-1.01
-37.8	313.5	0.735	0.598	0.0309	6.94	-1.29
-38.0	312.9	0.739	0.591	0.0312	7.13	-1.56
-38.2	311.8	0.748	0.578	0.0311	7.27	-1.74
-38.4	311.2	0.752	0.571	0.0316	7.54	-2.12
-38.5	310.7	0.756	0.565	0.0314	7.57	-2.15
-38.6	310.1	0.760	0.558	0.0316	7.75	-2.39
-38.7	309.6	0.764	0.551	0.0316	7.84	-2.51
-38.8	309.0	0.768	0.545	0.0322	8.15	-2.90
-38.9	308.5	0.772	0.538	0.0308	7.71	-2.33
-39.0	307.9	0.776	0.532	0.0307	7.72	-2.36
-39.1	307.4	0.780	0.525	0.0310	7.92	-2.61
-39.1	306.8	0.783	0.518	0.0307	7.91	-2.59
-39.2	306.3	0.787	0.512	0.0310	8.12	-2.85
-39.3	305.7	0.790	0.505	0.0300	7.80	-2.46
-39.4	305.2	0.794	0.499	0.0291	7.50	-2.07
-39.4	304.6	0.797	0.492	0.0292	7.65	-2.27
-39.5	304.1	0.800	0.485	0.0287	7.51	-2.08
-39.5	303.5	0.803	0.479	0.0287	7.60	-2.20
-39.6	303.0	0.806	0.472	0.0288	7.72	-2.35
-39.6	302.4	0.809	0.466	0.0284	7.62	-2.22
-39.7	301.9	0.812	0.459	0.0280	7.55	-2.13
-39.7	301.3	0.815	0.452	0.0272	7.29	-1.78
-39.7	300.8	0.818	0.446	0.0272	7.39	-1.91
-39.8	300.3	0.821	0.439	0.0269	7.33	-1.83
-39.8	299.7	0.823	0.433	0.0268	7.35	-1.86
-39.8	299.2	0.826	0.426	0.0264	7.28	-1.77
-39.8	298.7	0.829	0.419	0.0260	7.21	-1.66
-39.8	298.1	0.831	0.413	0.0260	7.27	-1.75
-39.8	297.6	0.834	0.406	0.0257	7.21	-1.67
-39.8	297.1	0.836	0.400	0.0258	7.32	-1.81
-39.8	296.5	0.838	0.393	0.0251	7.11	-1.53
-39.8	296.0	0.840	0.386	0.0245	6.91	-1.24
-39.8	295.5	0.843	0.380	0.0245	7.01	-1.38
-39.8	294.9	0.845	0.373	0.0244	7.02	-1.40
-39.8	294.4	0.847	0.367	0.0243	7.04	-1.43
-39.8	293.9	0.849	0.360	0.0234	6.75	-1.00
-39.7	293.4	0.851	0.353	0.0235	6.84	-1.15

TABLE I *continued*  
 Mariner 7, Phase Angle = 90.7

Lat.	Lon.	$\mu$	$\mu_0$	R	Pres.	Alt.
-39.7	292.9	0.853	0.347	0.0226	6.55	-.71
-39.7	292.3	0.854	0.340	0.0226	6.60	-.78
-39.6	291.8	0.856	0.334	0.0222	6.52	-.66
-39.6	291.3	0.858	0.327	0.0219	6.42	-.51
-39.5	290.8	0.860	0.320	0.0218	6.46	-.57
-39.5	290.3	0.861	0.314	0.0217	6.49	-.61
-39.4	289.8	0.863	0.307	0.0217	6.54	-.70
-39.4	289.3	0.864	0.300	0.0214	6.52	-.67
-39.3	288.8	0.866	0.294	0.0210	6.39	-.46
-39.3	288.3	0.867	0.287	0.0206	6.29	-.30
-39.2	287.8	0.868	0.281	0.0202	6.19	-.14
-39.1	287.3	0.869	0.274	0.0193	5.84	0.45
-39.0	286.8	0.871	0.267	0.0190	5.79	0.53
-39.0	286.3	0.872	0.261	0.0182	5.47	1.10
-38.9	285.8	0.873	0.254	0.0178	5.36	1.30
-38.8	285.3	0.874	0.248	0.0174	5.27	1.47
-38.7	284.8	0.875	0.241	0.0167	5.03	1.93
-38.6	284.3	0.876	0.234	0.0167	5.09	1.82
-38.5	283.8	0.877	0.228	0.0162	4.93	2.13
-38.4	283.4	0.877	0.221	0.0163	5.03	1.94
-38.3	282.9	0.878	0.215	0.0161	5.00	1.99
-38.2	282.4	0.879	0.208	0.0157	4.92	2.15
-38.1	281.9	0.879	0.202	0.0153	4.76	2.48

small value of  $k$  for this region. In the Hellas data obtained for the latitude and longitude range from  $-39^{\circ}6'$ ,  $291^{\circ}3'$  to  $-38^{\circ}1'$ ,  $281^{\circ}9'$  the Minnaert parameters were  $k = 0.83 \pm 0.04$  and  $R_0 = 0.055$ . A summary of ultraviolet Minnaert parameters is given in Table II.

Due to the large phase angles of the Mariner observations compared with ground-based observations, an exact comparison of the 3050 Å reflectances is not possible. Excluding unusual photometric properties, it is expected that the Earth-based measurements of the geometric albedo should be of the same order as the Minnaert constant,  $R_0$ , for the range of  $k$  values found. Earth-based data obtained by Irvine *et al.* (1968) indicate an average geometric albedo  $\sim 0.05$  at 3050 Å. Earth-based rocket data obtained in the 2550–3300 Å wavelength region by Broadfoot and Wallace (1970) give a geometric albedo  $\sim 0.09$  at 3050 Å. In this experiment, the Martian polar caps were included in the instrument field of view. A part of the intensity measured by Broadfoot and

Wallace may be attributed to the considerably brighter polar cap which has the effect of bringing their observations into closer agreement with the Mariner ultraviolet spectrometer results. The Mariner data indicate that the combination of desert reflectance, showing a monotonic increase in reflectance with decreasing wavelength, combined with a polar cap reflectance, with the broad ozone absorption centered at 2550 Å (Barth and Hord,

TABLE II  
 MINNAERT PARAMETERS

UVS data	$k$	$R_0$
Mariner 6 Aurorae Sinus, Margaritifer Sinus	$0.71 \pm 0.02$	0.037
Mariner 6 Deucalionis Regio	$0.69 \pm 0.06$	0.031
Mariner 7 Deucalionis Regio, Pandora Fretum	$0.31 \pm 0.01$	0.022
Mariner 7 Hellas	$0.83 \pm 0.04$	0.055

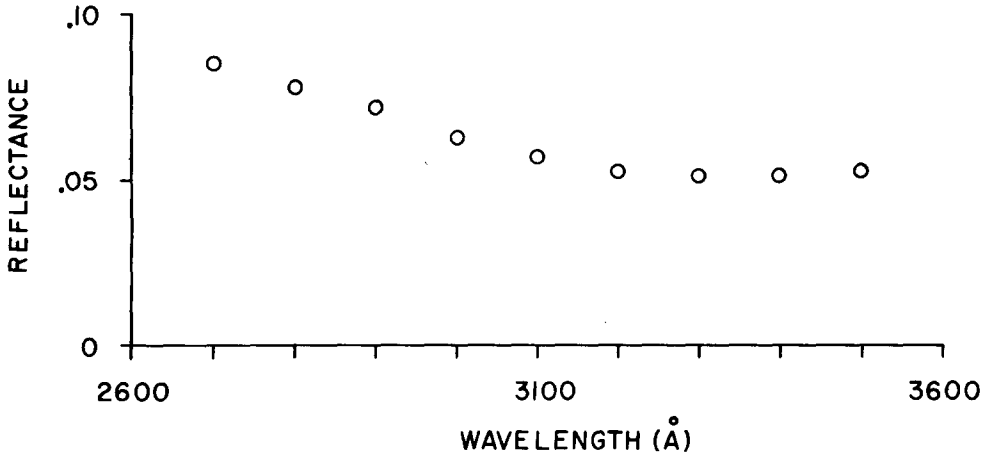


FIG. 4. Mariner 7 Mars reflectance as a function of wavelength obtained at latitude  $-19^{\circ}8$  and longitude  $353^{\circ}8$ , with  $\mu_0 = 0.971$ ,  $\mu = 0.225$ , and a phase angle of  $46^{\circ}3$ . The data points obtained every  $4.3 \text{ \AA}$  at a resolution of  $20 \text{ \AA}$  have been calibrated and divided by the solar flux, and are presented here at  $100 \text{ \AA}$  resolution consistent with the  $3050 \text{ \AA}$  reflectance data.

1971), would tend to give the constant reflectance as a function of wavelength observed by Broadfoot and Wallace. An earlier rocket experiment performed by Evans (1965) seems to qualitatively match the spectral shape observed by the Mariner spectrometer for the nonpolar regions of Mars. Evans' experiment used photographic methods while Broadfoot and Wallace used photoelectric detection as did the Mariner ultraviolet spectrometer. Results from the Orbiting Astronomical Observatory (OAO) ultraviolet experiment

give geometric albedos of  $0.0401$  at  $3215 \text{ \AA}$  and  $0.0428$  at  $2800 \text{ \AA}$  (Caldwell, 1970) using photoelectric detection methods.

#### SPECTRAL REFLECTANCE

Analysis of the Mariner ultraviolet spectrometer (UVS) data has shown that the illuminated disk of Mars has two characteristic ultraviolet spectral reflectances. These two spectral types, associated with the polar and nonpolar regions of the planet, have been discussed (Barth and Hord, 1971).

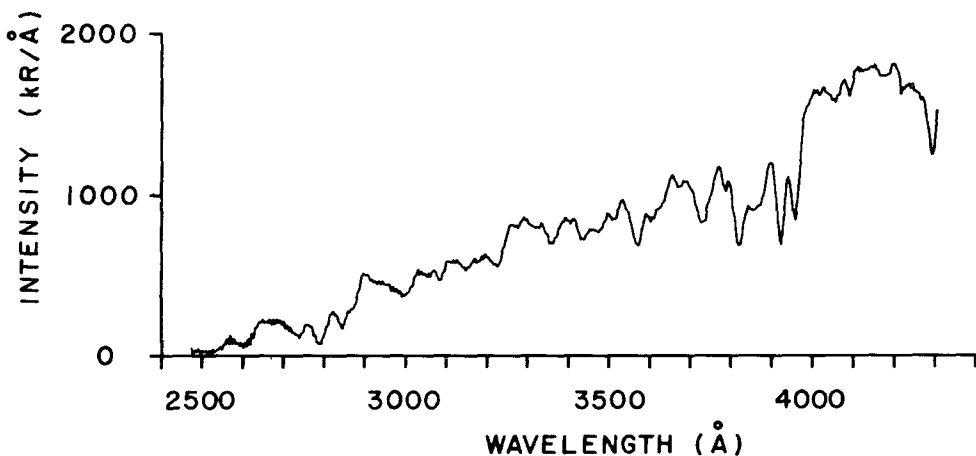


FIG. 5. Mariner 7 spectrum obtained with the spectrometer field of view including the bright limb of Mars. This spectrum was obtained at latitude  $-29^{\circ}$  and longitude  $307^{\circ}$ , with a phase angle of  $46^{\circ}3$  and a solar incidence angle equal to  $55^{\circ}$ .

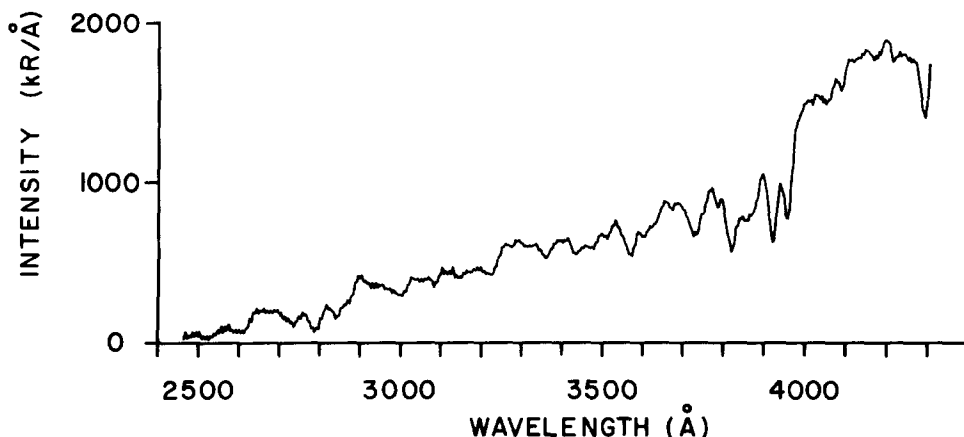


FIG. 6. Mariner 7 spectrum obtained at latitude  $-39^{\circ}0$  and longitude  $286^{\circ}8$ , with  $\mu_0 = 0.267$ ,  $\mu = 0.871$ , and a phase angle of  $90^{\circ}7$ .

Figure 4 shows the nonpolar Mars reflectance in the wavelength region from 2600 to 3600 Å, obtained by dividing a calibrated spectrum of Mars by the solar flux. In this wavelength interval, each of the 400 nonpolar spectra has the same basic spectral shape as shown in Fig. 4. Due to the large variation in the solar flux over the long wavelength channel (1900-

4300 Å), the instrument sensitivity was set to cause a full-scale measurement at about 3600 Å for most of the spectra obtained when observing the illuminated disk of Mars. This was done in order to obtain necessary sensitivity at shorter wavelengths. However, several spectra were obtained which were completely on scale throughout the spectral range 2500 to

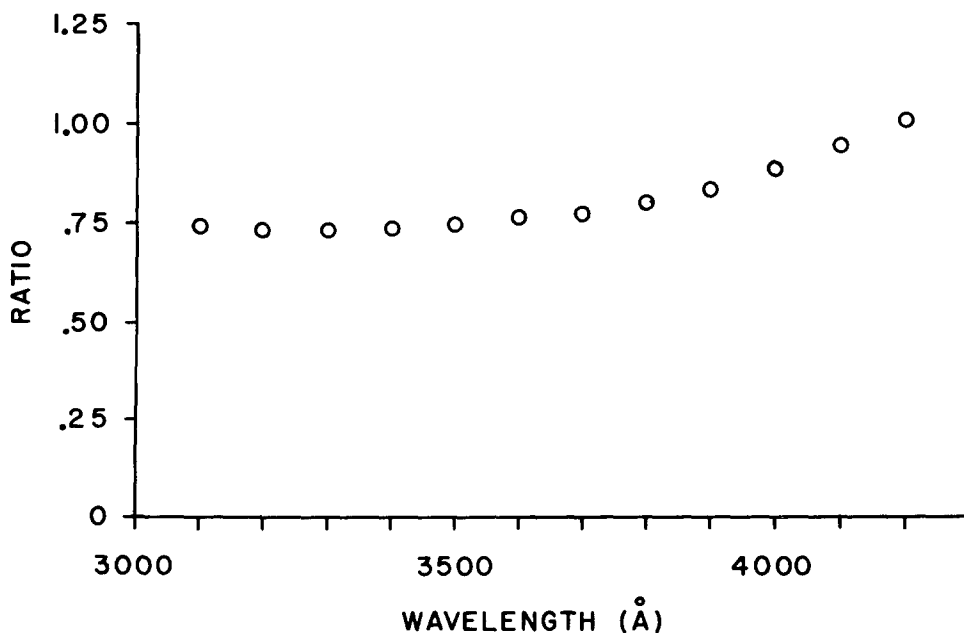


FIG. 7. Ratio of terminator to limb intensities obtained by dividing the spectrum in Fig. 6 by that in Fig. 5.

4300 Å. Figure 5 shows one of several ultraviolet spectra measured with the field of view of the instrument crossing the bright limb of Mars. In this particular geometry the long dimension of the UVS slit made an angle of  $55^\circ$  with the tangent to the limb and the field of view is only partially filled with the bright disk of Mars. This measurement at the bright limb with the field of view underfilled allowed an on-scale (at all wavelengths) spectrum to be obtained at the bright limb. Figure 6 shows one of the spectra taken near the evening terminator which are also fully on-scale due to the decreased solar illumination. Figure 7 shows the reflectance near the terminator relative to the bright limb reflectance and was obtained by dividing the spectrum in Fig. 6 by the Fig. 5 spectrum. A similar relative spectral reflectance is obtained by dividing any of the spectra taken near the terminator by any of the limb spectra. The spectral shapes are very nearly identical shortward of about 3600 Å and show the characteristic shape of the other nonpolar spectra. Longward of 3500 Å the terminator to limb intensity ratio increases monotonically, with wavelength, and illustrates the different photometric properties in this wavelength region. The terminator spectrum was obtained in the visually bright Hellas region which accounts for the increase in ratio at longer wavelengths.

#### PHOTOMETRIC MODEL

In the following analysis, Mariner 6 and 7 infrared spectrometer pressure data (Herr *et al.*, 1970) are combined with ultraviolet data in order to give a more realistic model of the 3050 Å reflectance of Mars. The ultraviolet reflectivity is assumed to consist of two components; an atmospheric part,  $(p/4)(\tau/\mu)$ , and a ground contribution,  $R_0\mu_0^k\mu^{k-1}$ . For the atmospheric part,  $p$  is the atmospheric scattering phase function,  $\tau$  is the vertical scattering optical depth, and  $\tau/\mu$  is the optical depth along the instrument line of sight. The phase function,  $p$ , depends upon the scattering angle,  $\zeta$ , which is the supplement of the phase angle. In the factor  $\tau/\mu$ ,  $1/\mu$  is

the airmass along the instrument line of sight. Near the bright limb of the planet, where the emission angle was large, the airmass is better represented by the more accurate Chapman function (see e.g., Hord *et al.*, 1970). In this discussion, the airmass will be represented by the secant factor,  $1/\mu$ , as this assumption does not alter the conclusions reached here. Pressure is directly proportional to column density and therefore to optical thickness for a homogeneous atmosphere, independent of temperature structure, so that

$$P = (P_0/\tau_0)\tau. \quad (3)$$

This assumption is made at the beginning and its accuracy will be evaluated at the end of the analysis. In the absence of a turbid atmosphere,  $\tau_0 = 0.032$  for  $P_0 = 6.0$  mb if the major constituent is carbon dioxide. Ground reflectance is represented by the Minnaert function in Eq. (2). The Minnaert parameters  $R_0$  and  $k$  are taken to be constant for this analysis, an assumption which can be tested *a posteriori*.

Atmospheric extinction is assumed to be due to scattering only so that pure absorption is neglected. Taking into account extinction and multiple scattering, the measured reflectance at 3050 Å is

$$R = f \left\{ \left( \frac{p}{4} \right) \left( \frac{\tau}{\mu} \right) \left[ \frac{1 - \exp(-\tau M)}{\tau M} \right] + R_0 \mu_0^k \mu^{k-1} \exp(-\tau M) \right\} \quad (4)$$

where  $[1 - \exp(-\tau M)]/\tau M$  and  $\exp(-\tau M)$  are attenuation factors associated with the atmospheric and surface parts of the reflectance. Total airmass,  $M$ , of the incident and outward optical paths is  $1/\mu_0 + 1/\mu$ . The multiple scattering factor,  $f$ , is a function of  $\mu$ ,  $\mu_0$ ,  $\zeta$ ,  $\tau$  as well as of the ground reflectance and the form of the phase function. Including the factor  $f$  makes Eq. (4) exact for the model selected. In practice, the magnitude of  $f$  can be estimated by comparison with exact solutions for simplified cases. For the small values of  $R_0$  and  $\tau$  encountered on Mars, the strongest dependence of  $f$  is on  $\tau$ . The factor  $f$  is greater than unity by an amount of order  $\tau$ . In this analysis  $f$  is taken to be

unity which causes the optical thickness to be overestimated by a small amount.

When Eq. (4) is solved for optical thickness and substituted into Eq. (3), the pressure as a function of the 3050 Å reflectance,  $R$ , is

$$P = \frac{P_0}{\tau_0 M} \ln \left[ \frac{R_0 \mu_0^k \mu^{k-1} - R_A}{R - R_A} \right], \quad (5)$$

where  $R_A$  is defined as  $p/(4\mu M)$ . Equation (5), with values for the constants  $\tau_0/P_0$ ,  $R_0$ ,  $k$ , and the phase function,  $p(\zeta)$ , constitute an algorithm for conversion of ultraviolet reflectance into pressure.

#### MARINER INFRARED AND ULTRAVIOLET PRESSURES

In the normalization of these data to a single occultation measurement (Barth and Hord, 1971), only one parameter can be specified, namely  $\tau_0 p(\zeta)/P_0$ , assuming no ground reflectance. Mariner infrared spectrometer pressure measurements (Herr *et al.*, 1970) provide the opportunity to understand more about the Mars physical parameters used in Eq. (5) and provide a test of the assumptions involved. The primary assumptions are a uniform ground reflectance and homogeneous scattering atmosphere.

A total of 23 infrared measurements from Mariner 6 and 35 from Mariner 7 were compared with corresponding ultraviolet measurements. Due to an offset in the fields of view of the two instruments, measurements of similar areas were made at subsequent times. The set of 58 infrared measurements which lie along the ultraviolet viewing path were selected for comparison. A corresponding set of 58 ultraviolet measurements, which correspond best in latitude and longitude with the infrared measurements, were also selected. Differences in spatial resolution and position observed on the planet have not been taken into account in this analysis. The long dimension of the infrared spectrometer slit, orientated perpendicular to the Sun, was 2°0 compared with 2°3 for the ultraviolet spectrometer. In the narrow dimension, the effective infrared field of

view was about half the size of the 0°23 ultraviolet dimension.

Using these 58 measurements the parameters  $\tau_0/P_0$ ,  $R_0$ ,  $k$ , and  $p(\zeta)$  for the scattering angles observed ( $\zeta = 89^\circ$ ,  $118^\circ$ ,  $134^\circ$ ) were varied in order to minimize the root mean square (rms) error defined by

$$\text{rms} = \left[ \frac{\sum_{i=1}^N (P_i^{(\text{UVS})} - P_i^{(\text{IRS})})^2}{N} \right]^{1/2}, \quad (6)$$

where  $P_i^{(\text{UVS})}$  and  $P_i^{(\text{IRS})}$  are the ultraviolet, Eq. (5), and infrared pressure measurements. Using nonlinear least squares techniques, the sensitivity of the rms error to each of the parameters of Eq. (5) could be tested. With this procedure the phase function and optical depth parameters were not well separated and the Minnaert parameter,  $k$ , did not have a strong effect on the rms error. The parameters obtained by this analysis were  $\tau_0 p(89^\circ)/P_0 = 0.0111$ ,  $p(118^\circ)/p(89^\circ) = 0.94$ ,  $p(134^\circ)/p(89^\circ) = 1.18$ ,  $R_0 = 0.015$ , and  $k \sim 1$ . This choice of parameters gave an rms error of 9% taking into account the degrees of freedom used in specifying five parameters. The agreement is good considering that pressure measurements used in this analysis varied by more than a factor of two. On a large scale, the agreement between the ultraviolet and infrared techniques is good, with the exception of the swath near Aurorae Sinus. It is notable that this is a region where chaotic terrain was observed by the Mariner television experiment (Sharp *et al.*, 1971). This is also the region noted by Neugebauer *et al.* (1971), where the observed albedo did not give the predicted surface temperature, as measured by the Mariner 6 infrared radiometer experiment. It is suggested that the assumption of homogeneity of ultraviolet atmospheric scattering may be violated here and may be related to the different appearance of this region. On a finer scale, differences between the ultraviolet and infrared observations are evident. Most notable is the Hellas region where the general trends of the ultraviolet and infrared data agree but where infrared pressures show much larger fluctuations in the terrain than is seen in

the ultraviolet. Ultraviolet pressures determined from Eq. (5) are listed in Table I. A total of 337 pressure measurements were made.

The inability to separate phase function and optical depth normalizations results from the small optical depth of the scattering atmosphere. A small optical depth causes the attenuation factors  $[1 - \exp(-\tau M)]/\tau M$  and  $\exp(-\tau M)$  to show only small variation for the range of air masses,  $M$ , involved. Large values of air mass were encountered near the bright limb while the ultraviolet spectrometer was changing from high gain, used for observing the Mars upper atmosphere, to low gain, for observations of the disk reflectance. Some observations made immediately after changing gain have larger air mass values and are consistent with the interpretation given here. However, the large variation of  $M$  over the instrument field of view near the bright limb, coupled with the strong effect of viewing geometry uncertainties, limits the sensitivity of these measurements for separation of optical thickness and phase function normalizations. In the 1971 Mariner 9 ultraviolet spectrometer experiment, observations will be made continuously across the bright limb at 4 km intervals with a resolution of the order of the lower atmosphere scale height. These limb data, coupled with observations nearer the terminator than were obtained by Mariner 6 and 7, can provide a basis for separating the  $\tau_0$  and  $p$  normalizations.

Lack of separation of  $\tau_0$  and  $p$  factors means that Eq. (5) can be expressed in a simpler way. Let the attenuation factors and multiple scattering factor,  $f$ , in Eq. (4) be replaced by average values  $\langle f \rangle$ ,  $\langle [1 - \exp(-\tau M)]/\tau M \rangle$ , and  $\langle \exp(-\tau M) \rangle$ . Results of this analysis indicate that  $\langle f \rangle \sim 1.1$ ,  $\langle [1 - \exp(-\tau M)]/\tau M \rangle \sim 0.9$ , and  $\langle \exp(-\tau M) \rangle \sim 0.8$ . If these corrections, which are of order unity, are assimilated so that  $R/\langle f \rangle \rightarrow R$ ,  $\tau \langle [1 - \exp(-\tau M)]/\tau M \rangle \rightarrow \tau$ , and  $R_0 \langle \exp(-\tau M) \rangle \rightarrow R_0$ , then Eq. (4) can be written

$$R = (p/4)(\tau/\mu) + R_0 \mu_0^k \mu^{k-1}. \quad (7)$$

This form displays the essential dependence of 3050 Å reflectance on atmospheric

scattering and ground reflectance. Equation (7) may be combined with the pressure relation, Eq. (3), giving

$$P = \frac{P_0}{\tau_0(p/4)} [R_\mu - R_0(\mu_0 \mu)^k]. \quad (8)$$

In this form, the coupling of the  $\tau_0$  and  $p$  normalizations is evident. If the phase function is normalized so that  $p(89^\circ) = 1$ , then  $\tau_0 = 0.068$  for  $P_0 = 6$  mb, which is about twice the scattering expected from a pure molecular atmosphere. Also note that the scattering phase function dependence,  $p(\zeta)$ , is more nearly isotropic than Rayleigh. This behavior is expected for particulate matter at the large scattering angles observed (see e.g. Deirmendjian, 1969). It is probable that the particulate scatterer has a forward peaked phase function so that  $p(89^\circ)$  is likely to be less than one in order to satisfy the phase function normalization relation

$$\frac{1}{4\pi} \int p(\zeta) d\Omega = \tilde{\omega}_0. \quad (9)$$

If the single scattering albedo,  $\tilde{\omega}_0$ , is less than unity, i.e. if pure absorption occurs, then  $p(89^\circ)$  may be even smaller. If  $p(89^\circ)$  is less than one, then  $\tau_0 > 0.068$ .

Apparent agreement of the ultraviolet measurements with infrared measurements suggests the assumption of a homogeneously mixed particulate scatterer is good. This implies that the particulate scatterers may have fairly long lifetimes in the Martian atmosphere and therefore puts a restriction on particle size (see e.g. Pollack and Sagan, 1969). Turbulent support may allow somewhat larger particles to contribute to a uniformly mixed scatterer. The monotonic increase in ultraviolet reflectance with decreasing wavelength noted earlier (Barth and Hord, 1971) implies a small scatterer.

If these two restrictions are placed on the particle size, i.e. if the particles must be large enough to have the observed phase function dependence but small enough to be suspended uniformly in the atmosphere, then the scatterer size may be comparable to the scattering wavelength, or about

0.3 $\mu$ . Another possibility that admits to a nonuniformly mixed scatterer is that larger particles account for the scattering and are preferentially stirred up for short times in the topographically low places on Mars.

An atmospheric spectral feature observed by the Mariner infrared spectrometer and identified as a silicate material (Herr and Pimentel, 1969) may be the nonmolecular scatterer observed in the ultraviolet. The limb haze observed by the Mariner television experiment does not appear homogeneous (Leovy *et al.*, 1971) and is difficult to reconcile with the ultraviolet data (Cutts, 1971).

The concept of measuring surface pressure is based upon measured ultraviolet intensity being dominated by scattering from an optically thin atmosphere against a small surface background. This possibility has been considered earlier by Evans (1965), Pollack (1967), and Sagan and Pollack (1966, 1968).

#### ALTITUDE ZERO

Although pressure is the more fundamental measurement, relative altitudes can be inferred from the ultraviolet data if some assumptions are made about atmospheric temperature structure. Belton and Hunten (1971) and Herr *et al.* (1970) have discussed the use of simple isothermal models in making pressure-to-altitude conversions. Herr *et al.* chose a single effective isothermal temperature, while Belton and Hunten adopted an isothermal model with variable effective temperature in order to better represent latitudinal temperature variation. The simpler conversion has been used here with a single effective isothermal temperature of 190°K corresponding to a 10km scale height. If the true Martian atmosphere is more nearly adiabatic with a 5°K/km lapse rate (Belton and Hunten, 1971) then an isothermal average model gives relative altitudes which are in error by  $\lesssim 10\%$  for the range of pressures encountered.

These authors have selected a value near the mean Mars pressure for their altitude zero. Herr *et al.* (1970) selected 6.0mb for

their altitude zero while Belton and Hunten (1971) selected 5.5mb. It is suggested that the selection of a normalization parameter such as this be chosen to convey physically useful information. The physically useful normalization or choice of zero altitude on the Earth is sea level. Barth (1971) has suggested that a meaningful normalization on Mars is to choose zero altitude to occur at the triple point-pressure of water,  $P_0 = 6.105$ mb. With this selection, liquid water is immediately precluded at all altitudes greater than zero. Water may exist at altitudes less than zero if the temperature is greater than 0°C and equilibrium conditions are reached. If Mars pressure is constant over geologic time, this would provide a unique pressure-altitude conversion reference point.

#### SUMMARY AND COMPARISON WITH OTHER MEASUREMENTS

Table III shows the subset of Mariner ultraviolet and infrared spectrometer data that were compared. Figures 8, 9, and 10 show the infrared pressures from Table III and the complete set of ultraviolet pressures determined from the comparison in Table I. Table IV lists the Mariner infrared and ultraviolet pressure data obtained north of Aurorae Sinus. As was the case in Table III, only the subset of data points which correspond closely in latitude and longitude are given. The anomalous region where the ultraviolet and infrared intercomparison breaks down, is evident in the left-hand side of Fig. 10. The primary effect of the solution for five parameters, which minimize the root mean square difference between ultraviolet and infrared measurements, is the gross shifting of the ultraviolet vertical scale in Figs. 8, 9, and 10. A residual rms error of 9% is quite small considering the number of components. If the sources of error are uncorrelated, it is correct to infer that errors due to: (1) relative ultraviolet reflectance, (2) infrared spectrometer pressures, (3) field of view differences, (4) assumption of uniform ground reflectance, and (5) assumption of a homogeneous scattering atmosphere, all introduce an error less than 9%.

TABLE III  
MARINER 6, PRESSURE COMPARISON (in mb)

P(UVS)	Lat.	Lon.	P(IRS)	Lat.	Lon.	Difference
6.23	3.3	21.9	6.23	2.7	21.9	0
6.58	2.7	20.6	6.45	2.1	20.7	0.13
6.42	2.4	19.7	5.92	1.7	19.6	0.50
5.71	1.8	18.5	6.50	1.1	18.3	-0.79
5.91	.8	16.0	6.15	0.2	15.9	-0.24
6.17	.4	14.7	6.32	-0.3	14.7	-0.15
6.07	.0	13.5	6.16	-0.7	13.4	-0.09
5.63	-.4	12.3	5.89	-1.0	12.2	-0.26
5.97	-.8	11.1	5.82	-1.4	11.0	0.15
7.04	-1.4	8.8	5.82	-2.0	8.6	1.22
4.79	-14.3	37.8	4.63	-13.3	38.1	0.16
4.77	-15.0	35.6	4.54	-14.2	35.2	0.23
5.99	-16.5	29.8	5.27	-15.7	30.0	0.72
5.77	-16.8	13.3	5.67	-16.2	13.2	0.10
5.48	-17.0	11.5	5.46	-16.5	11.4	0.02
5.41	-17.2	9.9	5.46	-16.7	9.7	-0.05
5.45	-17.5	6.6	5.51	-17.0	6.4	-0.06
5.28	-17.6	4.5	5.71	-17.1	4.7	-0.43
5.05	-17.8	1.5	4.96	-17.3	1.6	0.05
5.26	-17.8	359.6	4.95	-17.3	359.7	0.31
4.20	-17.8	355.3	4.66	-17.3	355.2	-0.46
4.44	-17.8	354.0	4.66	-17.3	353.7	-0.22
4.28	-17.6	350.8	4.70	-17.1	350.8	-0.42
4.88	-43.8	41.0	6.26	-47.2	41.4	-1.38
5.04	-44.6	40.1	5.01	-48.3	40.0	0.03
5.55	-47.1	37.2	5.59	-50.6	37.4	-0.04
5.80	-47.9	36.2	6.07	-51.6	36.1	-0.27
6.46	-49.0	34.9	6.43	-52.7	34.8	0.03
6.77	-50.1	33.5	5.50	-53.7	33.4	1.27
6.61	-51.2	32.1	5.29	-54.7	32.1	1.32
6.53	-53.3	29.4	5.48	-56.7	29.5	1.05
6.73	-54.3	28.0	5.49	-57.7	28.1	1.24
6.49	-55.3	26.7	6.74	-58.6	26.7	-0.25
6.67	-56.2	25.3	6.38	-59.6	25.3	0.29
7.08	-57.2	23.9	6.72	-60.5	23.9	0.36
4.62	-24.1	349.8	4.91	-26.4	349.7	-0.29
4.61	-26.4	347.4	4.75	-28.3	347.7	-0.14
4.63	-28.4	345.2	4.42	-30.0	345.7	0.21
4.53	-29.0	344.5	4.32	-31.6	343.8	0.21
4.22	-32.7	339.8	4.49	-34.3	340.0	-0.27
4.30	-33.6	338.6	4.16	-35.6	338.1	0.14
4.29	-35.2	336.0	4.19	-36.7	336.2	0.10
4.34	-36.3	334.1	4.34	-37.7	334.4	0
4.30	-37.3	332.3	4.05	-38.7	332.5	0.25
4.12	-39.1	328.5	4.22	-40.4	328.7	-0.10
4.37	-39.8	326.7	4.26	-41.2	326.8	0.11
4.69	-40.6	324.9	4.83	-41.9	324.9	-0.14
7.71	-38.9	308.5	6.57	-40.3	308.6	1.14
7.91	-39.1	306.8	6.55	-40.6	306.8	1.36
7.72	-39.6	303.0	7.59	-41.0	302.8	0.13
7.29	-39.7	301.3	7.10	-41.1	301.4	0.19
7.28	-39.8	299.2	8.16	-41.2	299.2	-0.88
7.21	-39.8	297.6	7.60	-41.2	297.5	-0.39
6.91	-39.8	296.0	6.08	-41.2	295.7	0.83
6.60	-39.7	292.3	6.77	-41.0	292.2	-0.17
6.49	-39.5	290.3	6.77	-40.9	290.5	-0.28
6.39	-39.3	288.8	7.00	-40.7	288.8	-0.61
5.84	-39.1	287.3	6.59	-40.5	287.1	-0.75

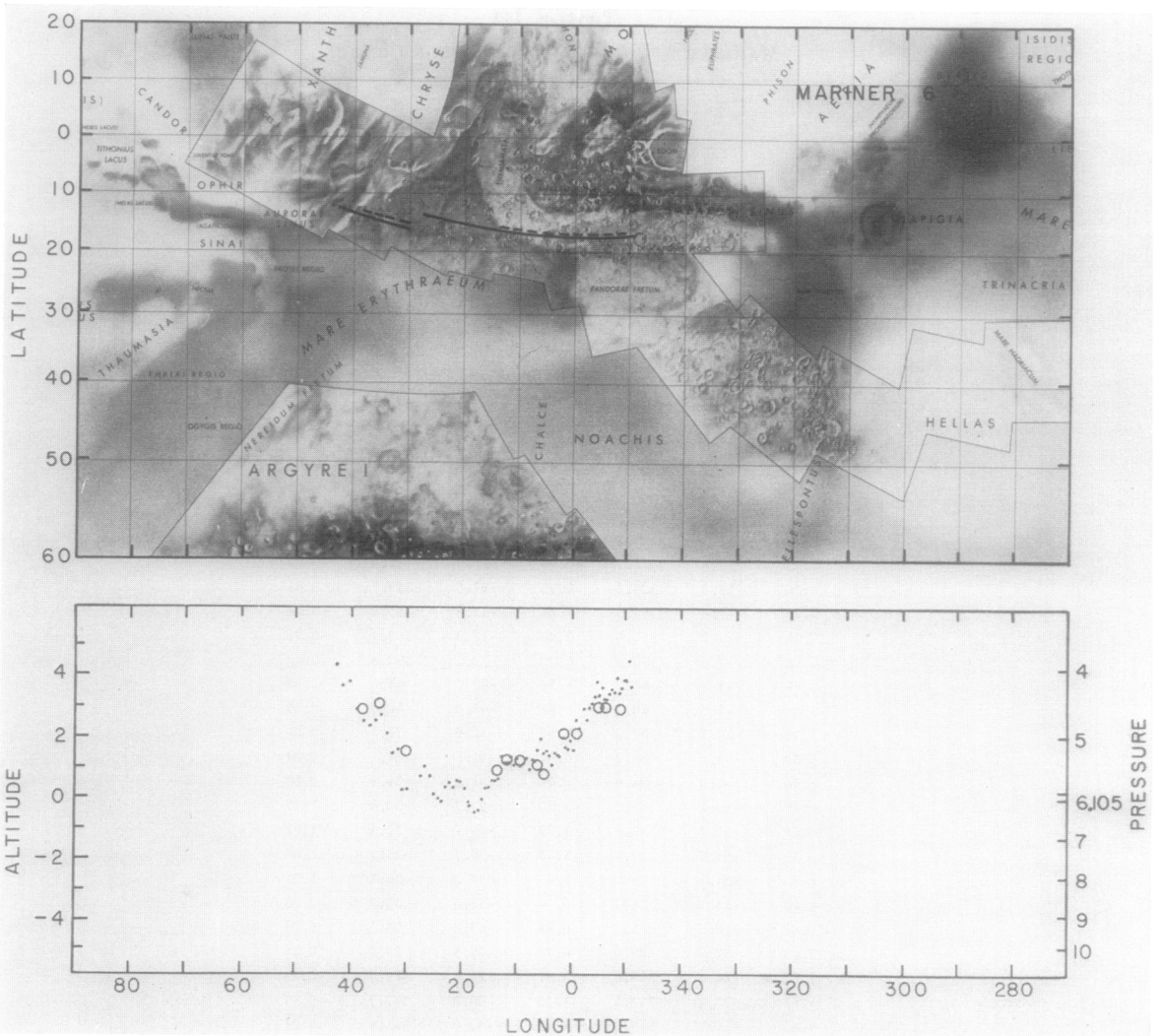


FIG. 8. Mariner 6 ultraviolet and infrared spectrometer pressures. The path of the center of the infrared spectrometer field of view across Mars is indicated by dashed lines and circles designate pressure measurements. Only that part of the infrared data which overlaps with ultraviolet measurements is shown. The path of the center of the ultraviolet spectrometer field of view across Mars is indicated by solid lines and pressure measurements are designated by dots. The Barth pressure normalization has been used so that zero altitude occurs at the triple point pressure of water.

Table V gives a comparison of  $\text{CO}_2$  pressures determined by Belton and Hunten (1971). Their measurements are based upon Earth-based measurement of the  $1\mu$  band of  $\text{CO}_2$  during the 1969 opposition. Figures 11 and 12 show the locations of the Belton and Hunten measurements and the comparison pressures listed in Table V. The projected field of view for these measurements was 800km

square or about  $13^\circ$  of latitude or longitude at the equator. Points in Table V were generated by simply averaging the  $\text{CO}_2$  pressures in a box of  $20^\circ$  longitude and  $20^\circ$  latitude centered at the locations where Mariner ultraviolet measurements were made. A subset of these averages were selected which showed the changes in  $\text{CO}_2$  pressure along the ultraviolet observation swaths. More sophisticated weighting

methods were tried and found not to materially improve or worsen the agreement. Reduction of box size to  $10^\circ$  reduces the number of comparison points significantly and does not show how well the general features of the two methods agree. The anomalous region north of Aurorae Sinus, noted in comparing the Mariner infrared and ultraviolet measurements, is again obvious in the left-hand side of Fig. 11. General agreement exists in this region between Earth-based data of Belton and Hunten and Mariner data of Herr *et al.*

Table VI compares altitudes obtained by the Haystack radar facility during the 1967 and 1969 oppositions (Pettengill *et al.*, 1969; Rogers *et al.*, 1970) with altitudes inferred from the Mariner ultraviolet pressure measurements. No scale adjustment has been used so that zero radar altitude corresponds to the triple point pressure of water,  $P_0 = 6.105$  mb. The assumption of an isothermal scale height of 10 km, used to convert the ultraviolet pressures to altitude, is adequate for this comparison as is seen in Fig. 13. A  $10^\circ$  latitude and longitude square centered at

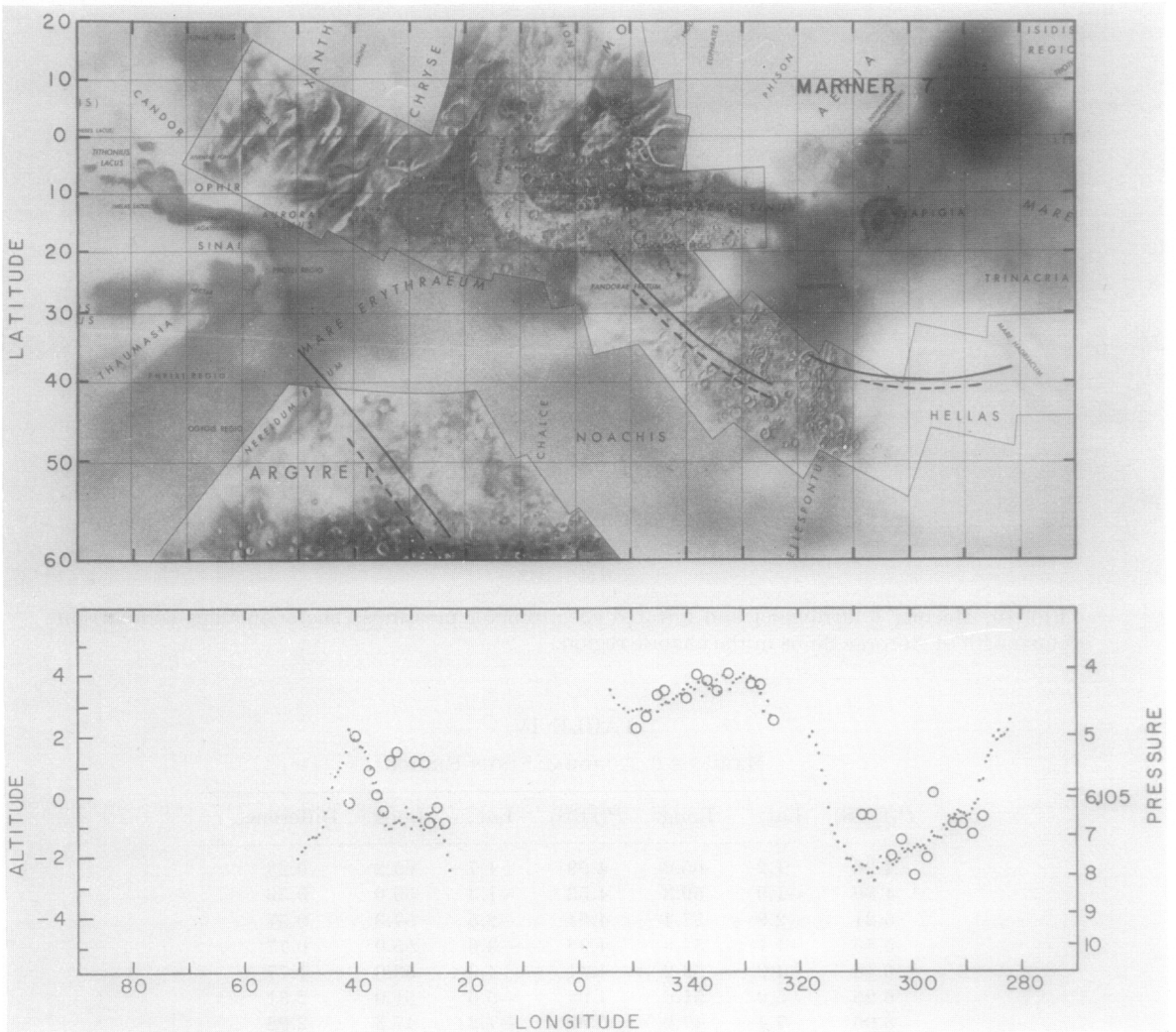


FIG. 9. Mariner 7 ultraviolet and infrared spectrometer pressures.

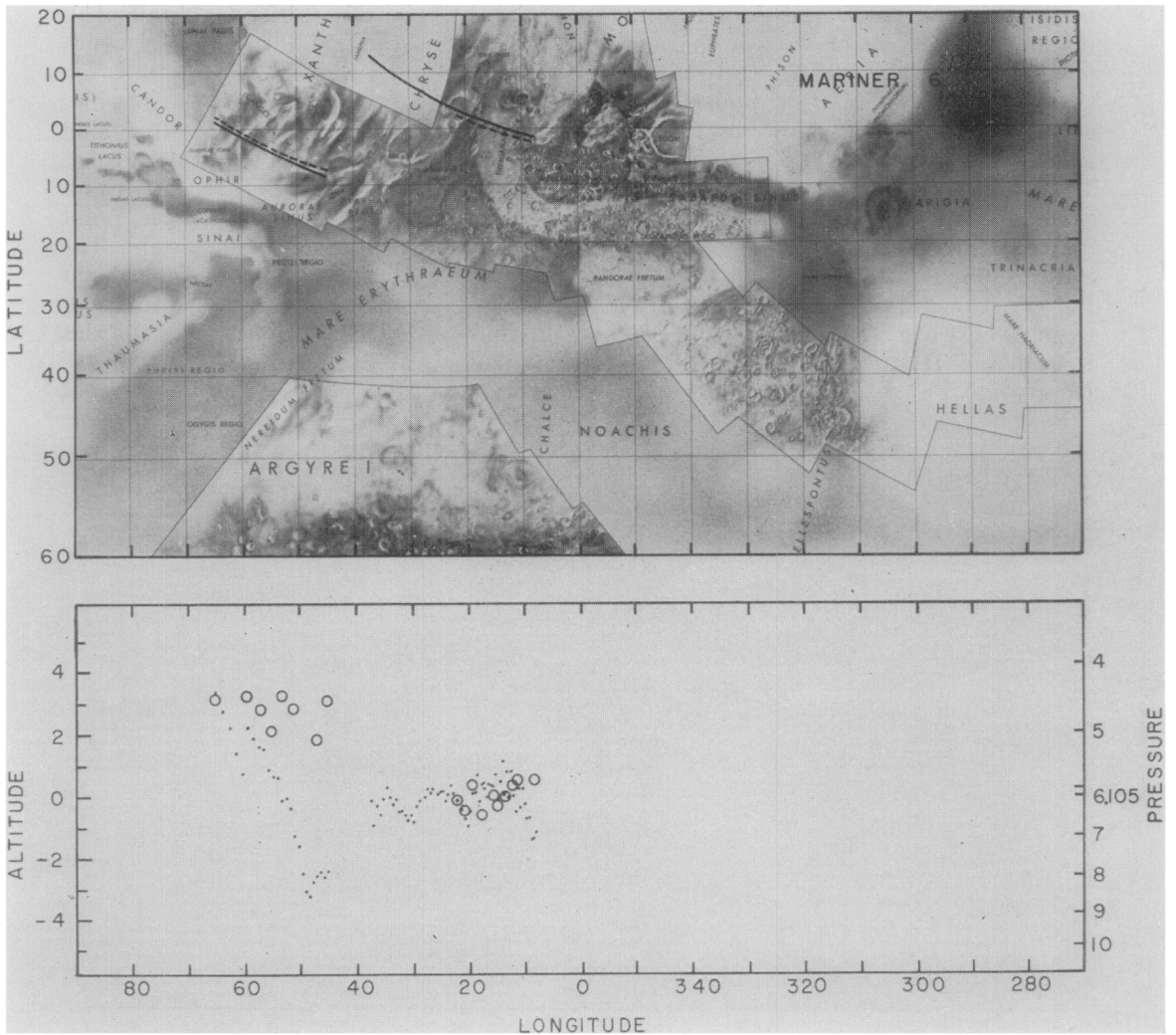


FIG. 10. Mariner 6 ultraviolet and infrared spectrometer pressures. The anomalous comparison occurs north of Aurorae Sinus in the chaotic region.

TABLE IV  
MARINER 6, AURORAE SINUS REGION

$P(\text{UVS})$	Lat.	Long.	$P(\text{IRS})$	Lat.	Long.	Difference
4.36	1.2	65.2	4.59	1.7	65.2	-0.23
4.89	-1.9	59.3	4.53	-1.3	59.6	0.36
5.21	-2.9	57.4	4.64	-2.5	57.3	0.57
5.73	-4.1	54.8	4.96	-3.6	55.0	0.77
6.18	-4.9	53.2	4.41	-4.6	53.0	1.77
6.95	-5.9	51.0	4.64	-5.6	51.0	2.31
8.06	-7.4	47.6	5.08	-7.2	47.3	2.98
7.93	-8.3	45.7	4.54	-8.0	45.6	3.39

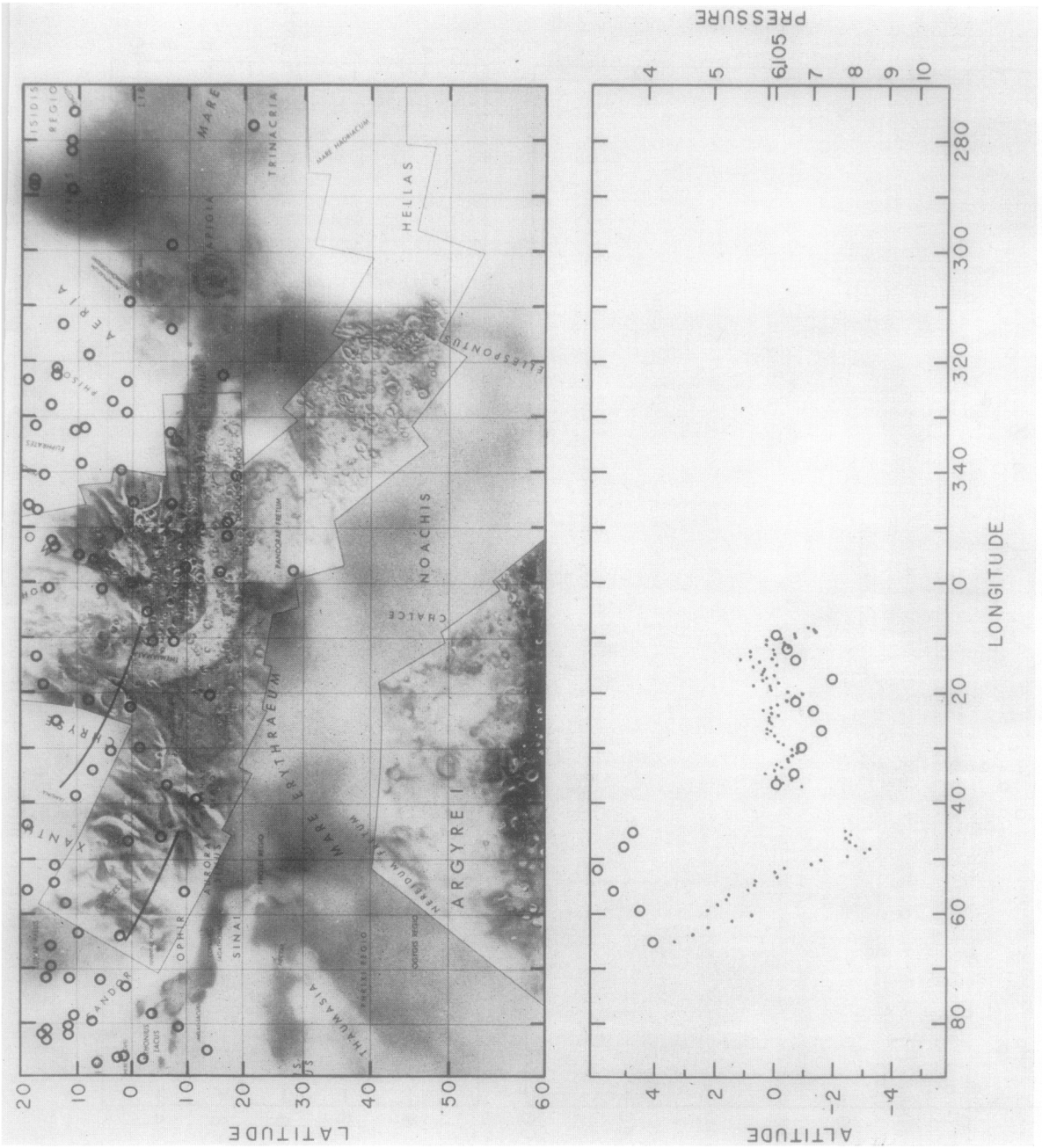


FIG. 11. Mariner 6 ultraviolet spectrometer pressures compared with Earth-based CO<sub>2</sub> results. Circles represent the locations on the base map. Infrared CO<sub>2</sub> pressures along the ultraviolet viewing path are shown as circles in the pressure graph.



TABLE V  
EARTH-BASED CO<sub>2</sub> PRESSURE

Lat.	Long.	$P(\text{UVS})$	$P(\text{CO}_2)$	Difference
1.2	65.2	4.36	4.06	0.30
-1.9	59.3	4.89	3.89	1.00
-3.7	55.6	5.61	3.56	2.05
-5.6	51.7	6.34	3.36	2.98
-7.4	47.6	8.06	3.68	4.38
-8.5	45.1	7.77	3.80	3.97
12.1	36.4	6.30	6.15	0.15
10.8	34.6	5.93	6.53	-0.60
7.7	29.8	6.64	6.70	-0.08
5.9	26.8	6.05	7.16	-1.11
4.0	23.2	5.90	6.97	-1.07
3.1	21.4	6.36	6.57	-0.21
1.5	17.6	5.88	7.44	-1.56
0.1	13.9	5.47	6.57	-1.10
-0.5	11.9	6.10	6.41	-0.31
-1.2	9.6	6.57	6.15	0.42
-13.5	40.3	4.20	4.49	-0.29
-15.5	33.5	4.98	4.44	0.54
-15.1	22.8	5.94	7.40	-1.46
-16.5	15.6	5.97	7.04	-1.07
-17.5	7.1	5.43	6.70	-1.27
-17.8	354.0	4.44	4.38	0.06

the ultraviolet measurement locations was used to generate radar altitudes, in the same manner used for the comparison with Earth-based CO<sub>2</sub> pressures. It is notable that a systematic difference in the two sets of measurements exists in the region extending from Chryse to the west edge of Meridiani Sinus. A systematic decrease in altitude from west to east across this region is not apparent in the ultraviolet measurements, or in either of the CO<sub>2</sub> pressure determinations.

The mean pressure based upon the 337 ultraviolet measurements is 5.8 mb. A mean value of 5.3 mb for the CO<sub>2</sub> pressure was found by Herr *et al.*, from the Mariner 6 and 7 infrared spectrometer data. A difference in mean pressure exists because observational swaths of the two Mariner instruments were only partially overlapping, even though the ultraviolet measurements were normalized to the infrared spectrometer data. Belton and Hunten report a mean pressure of 5.5 mb from their Earth-based CO<sub>2</sub> measurements.

If the Mars geometric albedo at 3050 Å

is calculated with the model (Eq. 4) to normalize the Mariner ultraviolet pressures to those of the infrared spectrometer, then

$$A = \frac{p(180^\circ)}{8} [1 - E_3(2\tau)] + 2R_0 E_{2k+2}(2\tau), \quad (10)$$

where  $p(180^\circ)$  is the phase function of  $180^\circ$  and  $E_3$  and  $E_{2k+2}$  are exponential integrals. The largest phase angle observed by Mariner ultraviolet spectrometer was  $134^\circ$  so that  $p(180^\circ)$  is unknown. If  $p(180^\circ) \sim 1$  and nominal values of  $R_0 = 0.015$ ,  $k \sim 1$ , and  $\tau = 0.066$  (corresponding to the average ultraviolet pressure of 5.8 mb) are substituted into Eq. (10), then  $A = 0.035$ . In this model, atmospheric scattering, which is accounted for by the first term in Eq. (10), contributes 0.026 with the remainder due to ground reflectance. The Caldwell (1970) analysis of the OAO ultraviolet spectrum of Mars attributes a sizeable portion of the Mars albedo to atmospheric scattering with the surface albedo contribution equal to 0.7 at 3215 Å and 0.5 at 2800 Å. Analysis of Earth-based polarization measurements by Ingersoll (1971) also indicates a large atmospheric contribution with surface

TABLE VI  
EARTH-BASED RADAR

Lat.	Long.	Alt. (UVS)	Alt. (Radar)	Difference
1.2	65.2	3.36	2.43	0.93
-0.2	62.5	2.21	2.20	0.01
-2.4	58.3	1.86	1.98	-0.12
12.6	37.0	-0.94	3.31	-4.25
11.3	35.2	-0.09	2.07	-2.16
10.1	33.5	-0.27	1.68	-1.95
8.0	30.3	-0.63	1.92	-2.55
7.0	28.8	-0.16	1.46	-1.62
6.2	27.3	0.21	1.02	-0.81
4.9	25.0	0.13	0.85	-0.72
3.8	22.7	0.08	0.59	-0.51
2.4	19.7	-0.51	-0.30	-0.21
1.5	17.6	0.38	-0.68	1.06
1.0	16.4	0.37	-1.15	1.52
0.0	13.5	0.06	-0.76	0.82
-0.7	11.5	-0.51	-0.61	0.10
-0.9	10.7	-0.38	-1.24	0.86
1.5	8.4	-1.38	-1.21	0.17

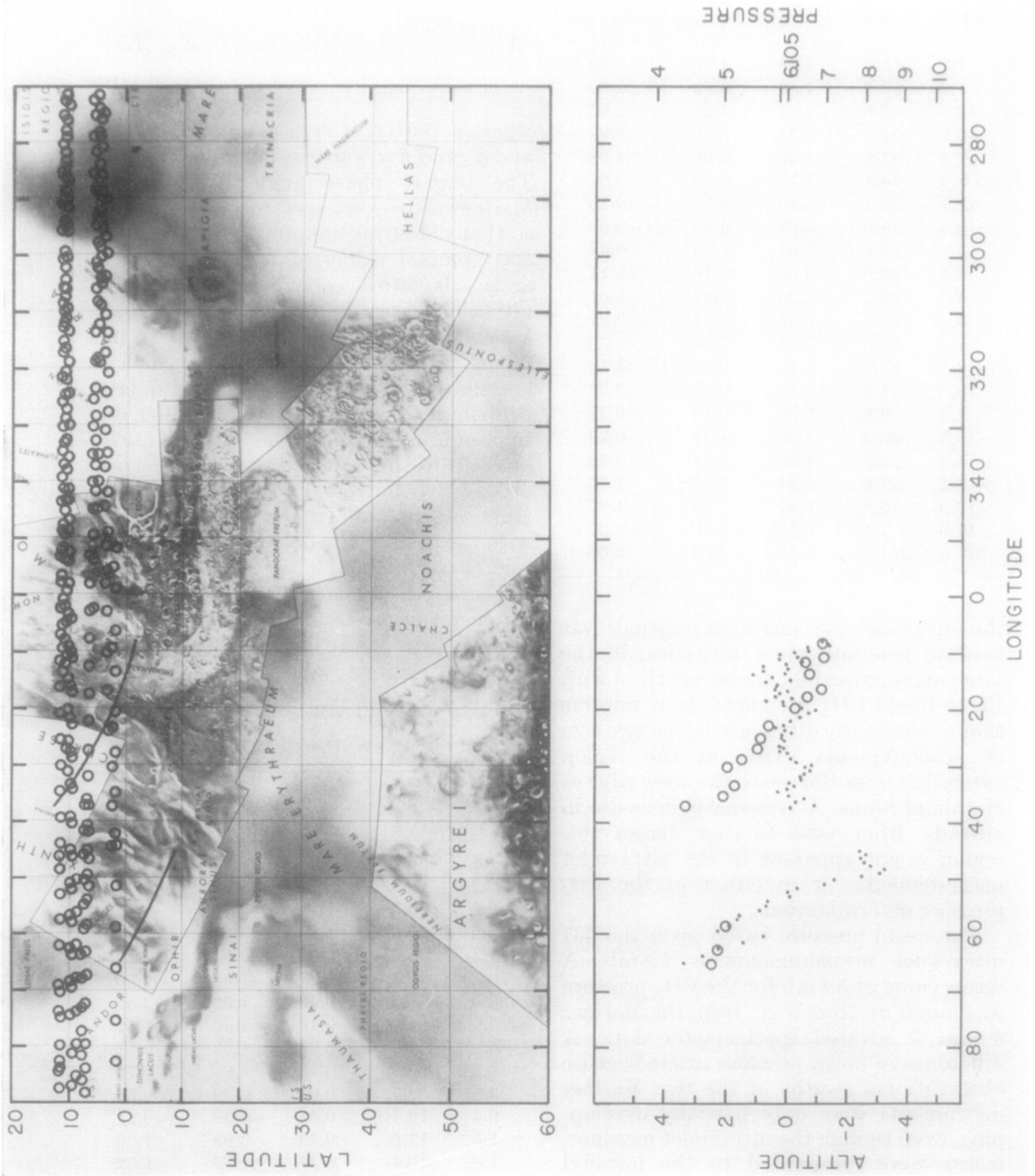


FIG. 13. Mariner 6 ultraviolet spectrometer altitudes compared with Haystack radar results. Circles show radar measure-

albedo contributing only 0.6 of the total planetary albedo at 3200 Å. It will be interesting to see if this model, which indicates that Mars has a very small ground reflectance near 3000 Å as well as a relatively large atmospheric signal, is confirmed by the Mariner 9 Mars orbiter.

#### ACKNOWLEDGMENTS

I wish to thank Dr. C. A. Barth for his valuable criticism of this work and, of course, his ultraviolet spectrometer data which makes this analysis possible. I would also like to thank Drs. Herr, Pimentel, Horn, Belton, and Hunten for the early availability of their data and valuable discussions. Karen Simmons and Lois Parmalee made valuable contributions in the preparation of the data.

This work was supported by NASA grant NGR-06-003-127.

#### REFERENCES

- BARTH, C. A. (1971). Private communication.
- BARTH, C. A., FASTIE, W. G., HORD, C. W., PEARCE, J. B., KELLY, K. K., STEWART, A. I., THOMAS, G. E., ANDERSON, G. P., AND RAPER, O. F. (1969). Mariner 6: Ultraviolet spectrum of Mars upper atmosphere. *Science* **165**, 1004-1005.
- BARTH, C. A., AND HORD, C. W. (1971). Mariner ultraviolet spectrometer: Topography and polar cap. *Science* **173**, 197-201.
- BARTH, C. A., HORD, C. W., PEARCE, J. B., KELLY, K. K., ANDERSON, G. P., AND STEWART, A. I. (1971). Mariner 6 and 7 ultraviolet spectrometer experiment: Upper atmosphere data. *J. Geophys. Res.* **76**, 2213-2227.
- BELTON, M. J. S., AND HUNTEN, D. M. (1971). The distribution of CO<sub>2</sub> on Mars: A spectroscopic determination of surface topography. *Icarus*, in press.
- BROADFOOT, L., AND WALLACE, L. (1970). Reflectivity of Mars, 2550-3300 Å. *Astrophys. J.* **161**, 303-307.
- CALDWELL, J. J. (1970). Ultraviolet Observations of Mars Made by the Orbiting Astronomical Observatory. Ph.D. Thesis, University of Wisconsin.
- CHANDRASEKHAR, S. (1960). "Radiative Transfer," p. 12. Dover, New York.
- CUTTS, J. A. (1971). Martian Spectral Reflectivity Properties from Mariner 7 Observations. Ph.D. Thesis, California Institute of Technology.
- CUTTS, J. A., DANIELSON, G. E., AND DAVIES, M. E. (1971). Mercator photomap of Mars. *J. Geophys. Res.* **76**, 369-372.
- DEIRMENDJIAN, D. (1969). "Electromagnetic Scattering on Spherical Polydispersions," pp. 256-271. American Elsevier, New York.
- EVANS, D. C. (1965). Ultraviolet reflectivity of Mars. *Science* **149**, 969-972.
- HERR, K. C., HORN, D., MCAFEE, J. M., AND PIMENTEL, G. C. (1970). Martian topography from the Mariner 6 and 7 infrared spectra. *Astron. J.* **75**, 833-894.
- HERR, K. C., AND PIMENTEL, G. C. (1969). Infrared absorption near three microns recorded over the polar cap of Mars. *Science* **166**, 496-499.
- HORD, C. W., BARTH, C. A., AND PEARCE, J. B. (1970). Ultraviolet spectroscopy experiment for Mariner Mars 1971. *Icarus* **12**, 63-77.
- INGE, J. L., CAPEN, C. F., MARTIN, L. J., FAURE, B. O., AND BAUM, W. A. (1971). A new map of Mars from planetary patrol photographs. *Sky and Telescope* **41**, 336-339.
- INGERSOLL, A. P. (1971). Polarization measurements of Mars and Mercury: Rayleigh scattering in the Martian atmosphere. *Astrophys. J.* **163**, 121-129.
- IRVINE, W. M., SIMON, T., MENZEL, D. H., CHARON, J., LECOMTE, G., GRIBOVAL, P., AND YOUNG, A. T. (1968). Multicolor photoelectric photometry of the brighter planets. II. Observations from Lehouga observatory. *Astron. J.* **73**, 251-264.
- LEIGHTON, R. B., HOROWITZ, N. H., MURRAY, B. C., SHARP, R. P., HERRIMAN, A. H., YOUNG, A. T., SMITH, B. A., DAVIES, M. E., AND LEOVY, C. B. (1969). Mariner 6 and 7 television pictures: Preliminary analysis. *Science* **166**, 49-67.
- LEOVY, C. B., SMITH, B. A., YOUNG, A. T., AND LEIGHTON, R. B. (1971). Mariner Mars 1969: Atmospheric results. *J. Geophys. Res.* **76**, 297-312.
- MINNAERT, M. (1941). The reciprocity principle in Lunar photometry. *Astrophys. J.* **93**, 403-410.
- NEUGEBAUER, G., MÜNCH, G., KIEFFER, H., CHASE, S. C. JR., AND MINER, E. (1971). Mariner 1969 infrared radiometer results: Temperature and thermal properties of Martian surface. *Astron. J.*, in **76**, 719-728.
- PANG, K., AND HORD, C. W. (1971). Mariner 7 ultraviolet spectrometer experiments: Photometric function and roughness of Mars' polar cap surface. *Icarus* **15**, 443-453.

- PEARCE, J. B., GAUSE, K. A., MACKAY, E. F., KELLY, K. K., FASTIE, W. G., AND BARTH, C. A. (1971). Mariner 6 and 7 ultraviolet spectrometers. *Appl. Optics*, **10**, 805-812.
- PETTENGILL, G. H., COUNSELMAN, C. C., RAINVILLE, L. P., AND SHAPIRO, I. I. (1969). Radar measurements of Martian topography. *Astron. J.* **74**, 461.
- POLLACK, J. B. (1967). Rayleigh scattering in an optically thin atmosphere and its application to Martian topography. *Icarus* **7**, 42-46.
- POLLACK, J. B., AND SAGAN, C. (1969). An analysis of Martian photometry and polarimetry. *Space Sci. Rev.* **9**, 243-299.
- ROGERS, A. E. E., PETTENGILL, G. H., SHAPIRO, I. I., ASH, M. E., AND COUNSELMAN, C. C. (1970). Radar Studies of Mars. Final Report, contract NAS 9-7830 to NASA.
- SAGAN, C., AND POLLACK, J. B. (1966). Elevation differences on Mars. *Smithsonian Astrophys. Obs. Spec. Rept.* **221**. Also *J. Geophys. Res.* **73**, 1373-1387 (1968).
- SHARP, R. P., SODERBLOM, L. A., MURRAY, B. C., AND CUTTS, J. A. (1971). The surface of Mars 2. uncratered terrains. *J. Geophys. Res.* **76**, 331-342.
- YOUNG, A. T., AND COLLINS, S. A. (1971). Photometric properties of the Mariner cameras and of selected regions on Mars. *J. Geophys. Res.* **76**, 432-437.